A new clinopyroxene-liquid barometer, and implications for magma storage pressures under Icelandic rift zones

DOI:
10.2138/am-2017-5968

Document Version
Accepted author manuscript

Revision 2

A New Clinopyroxene-liquid Barometer, and Implications for Magma Storage Pressures under Icelandic Rift Zones

David A. Neave[1*] and Keith D. Putirka[2]

[1]Leibniz Universität Hannover, Institut für Mineralogie, Callinstraße 3, 30167 Hannover, Germany

[2]Department of Earth and Environmental Sciences, California State University-Fresno, 2345 East San Ramon Avenue, MS/MH24, Fresno, California 93720, U.S.A.

*Corresponding author: Leibniz Universität Hannover, Institut für Mineralogie, Callinstraße 3, 30167 Hannover, Germany

Phone: +49 (0) 511 762-3222, Fax: +49 (0) 511 762-3045

Email: d.neave@mineralogie.uni-hannover.de

Revised manuscript for resubmission to *American Mineralogist*

November 2016

Number of words (main text only): 7694

David A. Neave d.neave@mineralogie.uni-hannover.de

Keith D. Putirka kputirka@csufresno.edu

Abstract

Pressure is one of the key variables that controls magmatic phase equilibria. However, estimating magma storage pressures from erupted products can be challenging. Various barometers have been developed over the past two decades that exploit the pressure-sensitive incorporation of jadeite (Jd) into clinopyroxene. These Jd-in-clinopyroxene barometers have been applied to rift zone magmas from Iceland, where published estimates of magma storage depths span the full thickness of the crust, and extend into the mantle. Tests performed on commonly used clinopyroxene-liquid barometers with data from experiments on H_2O-poor tholeiites in the 1 atm to 10 kbar range reveal substantial pressure-dependent inaccuracies, with some models overestimating pressures of experimental products equilibrated at 1 atm by up to 3 kbar. The pressures of closed-capsule experiments in the 1–5 kbar range are also overestimated, and such errors cannot be attributed to Na loss, as is the case in open furnace experiments. The following barometer was calibrated from experimental data in the 1 atm to 20 kbar range to improve the accuracy of Jd-in-clinopyroxene barometry at pressures relevant to magma storage in the crust:

$$\mathrm{P(kbar)} = -26.27 + 39.16\frac{\mathrm{T(K)}}{10^4}\ln\left[\frac{\mathrm{X_{Jd}^{cpx}}}{\mathrm{X_{NaO_{0.5}}^{liq}}\mathrm{X_{AlO_{1.5}}^{liq}}\left(\mathrm{X_{SiO_2}^{liq}}\right)^2}\right] - 4.22\ln\left(\mathrm{X_{DiHd}^{cpx}}\right) + 78.43\mathrm{X_{AlO_{1.5}}^{liq}} + 393.81\left(\mathrm{X_{NaO_{0.5}}^{liq}}\mathrm{X_{KO_{0.5}}^{liq}}\right)^2$$

This new barometer accurately reproduces its calibration data with a standard error of estimate (SEE) of ±1.4 kbar, and is suitable for use on hydrous and anhydrous samples that are ultramafic to intermediate in composition, though should be used with caution below 1100 °C and at oxygen fugacities greater than one log unit above the QFM buffer. Tests performed using with data from experiments on H_2O-poor tholeiites revealed that 1 atm runs were overestimated by less than the model precision (1.2 kbar); the new calibration is significantly more accurate than previous formulations. Many current estimates of magma storage pressures may therefore need to be reassessed. To this end, the new barometer was applied to numerous published clinopyroxene analyses from Icelandic rift zone tholeiites that were filtered to exclude compositions affected by poor analytical precision or collected from disequilibrium sector zones. Pressures and temperatures were then calculated using the new barometer in concert with equation 33 from Putirka (2008). Putative equilibrium liquids were selected from a large database of Icelandic glass

and whole-rock compositions using an iterative scheme because most clinopyroxene analyses were too primitive to be in equilibrium with their host glasses. High-Mg# clinopyroxenes from the highly primitive Borgarhraun eruption in north Iceland record a mean pressure in the lower crust (4.8 kbar). All other eruptions considered record mean pressures in the mid-crust, with primitive clinopyroxene populations recording slightly higher pressures (3.5–3.7 kbar) than evolved populations (2.5–2.8 kbar). Thus, while some magma processing takes place in the shallow crust immediately beneath Iceland's central volcanoes, magma evolution under the island's neovolcanic rift zones is dominated by mid-crustal processes.

Key words: thermobarometry; clinopyroxene-liquid equilibria; Iceland; magma plumbing

INTRODUCTION

Clinopyroxene-liquid Barometry—Background and Applications

Alongside composition, crystallinity, temperature and oxygen fugacity, pressure is one of the primary intensive variables that controls magmatic phase equilibria (Yoder and Tilley 1962; Blundy and Cashman 2008). This raises the possibility of estimating magma storage pressures using observed phase equilibria relations and information from other intensive variables. Indeed, determining magma storage pressures, and hence depths, is essential for various reasons. For example, understanding the distribution of magma storage depths within the lithosphere provides information about crustal formation mechanisms in both oceanic and continental settings (Henstock et al. 1993; Kelemen et al. 1997; Annen et al. 2006). Estimating pre-eruptive magma storage depths is also essential for integrating petrological records of magmatism with expressions of ongoing unrest such as seismicity, ground deformation and gas emission in volcanically active regions (Edmonds 2008; Sigmundsson et al. 2010; Tarasewicz et al. 2014). With the aim of improving the accuracy with which magma storage pressures can be estimated, we assessed the performance of various published clinopyroxene-liquid barometers. To anticipate our results, we find that some barometers overestimate reported experimental pressures at <7 kbar. We thus develop a new jadeite-in-clinopyroxene barometer optimized for use at crustal pressures on hydrous and anhydrous

compositions. We then recalculate storage pressures for a series of Icelandic rift tholeiites from which diverse clinopyroxene-liquid pressures have been reported in recent years.

The number of barometric tools available for estimating magma storage pressures has grown considerably over the past 25 years. Current barometric methods range from exploiting volatile solubility laws (e.g., Newman and Lowenstern 2002; Moore 2008) or equations of state (Hansteen and Klügel 2008) to determine melt and fluid inclusion entrapment pressures, through to calibrating pressure-sensitive phase equilibria relations using experimental data (e.g., Putirka 2008). However, these various barometric methods are subject to numerous assumptions and unavoidably return pressure estimates with considerable uncertainties. For example, while the solubilities of H_2O and CO_2 in silicate melts are generally well understood (Dixon and Stolper 1995; Lesne et al. 2011; Shishkina et al. 2014), many recent studies have demonstrated that interpreting melt inclusion entrapment pressures can be complicated by post-entrapment processes such as diffusive reequilibration, shrinkage bubble formation and the precipitation of solid carbon phases (Bucholz et al. 2013; Hartley et al. 2014; Moore et al. 2015; Wallace et al. 2015). Although condensed phase barometry (i.e., barometry based on solid-solid or solid-liquid phase equilibria) can avoid the challenges presented by melt and fluid inclusions, it is fundamentally limited in other ways. For example, determining magma storage pressures is complicated not only by the mostly small volume contrasts associated with most mineral-mineral or mineral-liquid equilibria, but also by the small number of phases present in many magmas (e.g., melt + olivine ± plagioclase ± clinopyroxene in the case of many mafic magmas; Grove et al. 1992), which limits the number of reactions available for barometric use.

Fortunately for igneous petrologists, the incorporation of jadeite ($NaAlSi_2O_6$; Jd) into clinopyroxene is strongly pressure dependent, with high Jd contents stabilized at high pressures as a result of the large partial molar volume change associated with the formation of the Jd component (Putirka et al. 1996; Holland and Powell 1998; Putirka 2016). About twenty years ago, Putirka et al. (1996) presented a series

of equations describing the pressure-dependent Jd-liquid (liq) reaction, as well as the strongly temperature-dependent Jd into diopside-hedenbergite ($Ca(Mg,Fe)Si_2O_6$; DiHd) and calcium Tschermak's component ($CaAlAlSiO_6$; CaTs) into DiHd exchange reactions. These thermobarometric equations were subsequently reformulated in 2003 to extend their applicability to felsic and hydrous systems(Putirka et al. 2003), before being reviewed further five years later (Putirka 2008).

Perhaps unsurprisingly, these clinopyroxene-liquid thermobarometers have now seen extensive use for some years. A far from exhaustive list of barometric studies that have used clinopyroxene-liquid equilibria would include the description of deep, multi-level magmatic differentiation under the Canary Islands (Hansteen et al. 1998; Klügel et al. 2005; Stroncik et al. 2009), as well as the identification and subsequent re-evaluation of deep fractionation recoded by high-Al clinopyroxene crystals in alkaline magmas from Haleakala, Hawaii (Chatterjee et al. 2005; Hammer et al. 2016). Clinopyroxene-liquid equilibria have also been used to define trans-crustal magma plumbing systems under Mt. Etna amongst other locations (Giacomoni et al. 2016). To improve the suitability of clinopyroxene-liquid thermobarometers for studying evolved alkaline systems, a series of recalibrated thermobarometric expressions have been developed and applied to Mt. Vesuvius and Campi Flegrei in Italy (Masotta et al. 2013), as well as to Nemrut in Turkey (Macdonald et al. 2015).

Clinopyroxene-liquid thermobarometers have also been applied to the products of several Icelandic eruptions. For example, clinopyroxene-liquid storage pressure from the primitive Borgarhraun lava in the on-axis Northern Volcanic Zone (NVZ) of Northern Iceland indicate that clinopyroxene crystallization occurred close to the Moho (>20 km; Maclennan et al. 2003a; Winpenny and Maclennan 2011). These high storage pressures are also consistent with phase equilibria experiments and estimates from olivine-plagioclase-augite-melt (OPAM) boundary barometry (Yang et al. 1996; Maclennan et al. 2012). In the southern, off-axis extension of Iceland's Eastern Volcanic Zone (sEVZ), a bimodal distribution of storage depths has been inferred for the 2010 Eyjafjallajökull-Fimmvörðuháls eruption, with the basalts erupted

from the flank thought to have been sourced from substantially greater depths (16–18 km) than the benmoreites erupted from the summit (2–5 km; Keiding and Sigmarsson 2012). Similar vertically extensive magma plumbing systems have also been inferred from the products of the neighboring Katla volcanic system (Budd et al. 2016).

The importance of mid-crustal storage has also been demonstrated in the products of the 1783–1784 Laki and 10 ka Grímsvötn tephra series eruptions from the on-axis portion of the Eastern Volcanic Zone (EVZ; Neave et al. 2013, 2015). However, these studies of the EVZ proper used substantially different approaches from those used in studies of the sEVZ. Firstly, instead of using the carrier melt as the equilibrium liquid for thermobarometric calculations, putative equilibrium liquids were selected from a large database of Icelandic glass and whole-rock analyses on the basis of being in Fe-Mg, Ti and CaTs component equilibrium with measured clinopyroxenes (e.g., Winpenny and Maclennan 2011). In other words, no *a priori* assumptions about which liquids would be in equilibrium with clinopyroxene crystals were made. Avoiding such assumptions was deemed to be essential because of the extensive disequilibrium within and between the different components of Icelandic magmas (Halldórsson et al. 2008; Maclennan 2008; Neave et al. 2014). For example, even though Keiding and Sigmarsson (2012) and Budd et al. (2016) performed thermobarometric calculations on clinopyroxene compositions in Fe-Mg equilibrium with co-erupted glass or whole-rock compositions, only the outermost rims of analyzed crystals may have been co-genetic with the melts that carried them to the surface; magma mixing could have decoupled earlier growth phases of such crystals from their equilibrium melts. Besides, even if a system establishes Fe-Mg exchange equilibrium, the equilibration of pressure-dependent NaAl-CaMg exchange is by no means guaranteed; different components may equilibrate at different rates. Filtering for Fe-Mg equilibrium alone may thus be an insufficient test for equilibrium in systems where mixing is prevalent (Zellmer et al. 2014). Moreover, Fe-Mg exchange is insensitive to the disequilibrium growth of clinopyroxene, and testing for equilibrium across multiple clinopyroxene components is probably more robust (Mollo et al. 2013a). Secondly, the accuracy of the barometric equations used in the EVZ studies

was tested by applying them to experiments on mafic compositions in the 1–7 kbar range. The pressures from experimental clinopyroxene-liquid pairs were generally found to exceed the pressures at which experiments were carried out, so empirical corrections were applied to the results of calculations performed in clinopyroxene from the Laki and 10 ka Grímsvötn tephra series eruptions (Neave et al. 2013, 2015).

The magnitudes of empirical corrections proposed by Neave et al. (2013, 2015) (−1.5 and −2.7 kbar respectively at a true pressure of 3 kbar) are comparable with the 2–3 kbar overestimation of most 1 atm experimental data noted by Putirka (2008) when testing various Jd-in-clinopyroxene barometers (Putirka et al. 1996, 2003). This overestimation was initially attributed to Na loss during open furnace experiments artificially shifting the equilibrium constant of Jd formation in favor of higher pressure estimates (Tormey et al. 1987; Putirka 2008). However, the persistence of this overestimation when barometers are applied to the products of higher pressure experiments carried out in closed capsules suggests that Na volatilization alone cannot account for the poor accuracy of Jd-in-clinopyroxene barometers at low pressures. Unfortunately, the tests carried out by Neave et al. (2013, 2015) are insufficient to evaluate the performance of currently available barometers robustly: they were performed using an incomplete experimental database that was not filtered for the attainment of clinopyroxene-liquid equilibrium. To provide more reliable evaluation of published barometers, we therefore carried out a series of tests on a much larger experimental database.

Evaluating the Performance of Published Clinopyroxene-liquid Barometers

When the first Jd-in-clinopyroxene barometer was proposed by Putirka et al. (1996), few high-temperature phase equilibria data were available for mafic systems above 1 atm and below 7 kbar—arguably, the pressure interval where most magma reservoirs are located (e.g., Singh et al. 2006; Cashman and Sparks 2013; Tarasewicz et al. 2014; Gudmundsson et al. 2016)—because of the experimental challenges of working under these conditions. Many 1 atm experiments carried out before the mid-1990s

also experienced Na loss, limiting their use in calibrating Jd exchange equilibria (Tormey et al. 1987). However, a range of technological developments over the past few decades have greatly expanded the number of low- to moderate-pressure (≤7 kbar) experiments available for calibrating and testing thermobarometers. Notable advancements include: introducing procedures for minimizing Na loss during open furnace experiments (Tormey et al. 1987; Yang et al. 1996); developing rapid quench devices for internally heated pressure vessels (IHPVs; Berndt et al. 2002; Holloway et al. 1992; Moore and Carmichael 1998); and modifying piston cylinder assemblies to achieve reproducible pressures when operating below 7 kbar (Moore et al. 2008).

Phase equilibria experiments from the following sources were thus compiled to evaluate published clinopyroxene-liquid barometers: Berndt et al. (2005), Botcharnikov et al. (2008), Grove et al. (1992), Husen et al. (2016), Thy et al. (2006), Toplis and Carroll (1995), Villiger et al. (2004, 2007), Whitaker et al. (2007, 2008) and Yang et al. (1996). We only include low-H_2O ($H_2O \leq 1$ wt.%) experiments that were carried out at ≤10 kbar with an fO_2 between the C-CO_2-CO buffer (i.e., in equilibrium with graphite capsules) and one log unit above the QFM buffer (QFM+1). These conditions encompass the anticipated magma storage conditions for tholeiitic basalts in oceanic settings (Michael 1995; Cottrell and Kelley 2011). They also exclude the oxidizing conditions (fO_2 > QFM+1) under which the presence of Fe^{3+} in clinopyroxene can stabilize an aegirine component ($NaFe^{3+}Si_2O_6$; Aeg) that complicates the solution of Na into pyroxene, with an unknown impact on the true Jd fraction, compared to that calculated from major element oxide data (Blundy et al. 1995). Furthermore, only clinopyroxene-liquid pairs with $K_{d\,Fe-Mg}^{cpx-liq}$ values within 20% of equilibrium values calculated using equation 35 from Putirka (2008) were considered. The compiled experimental data are provided in the electronic appendix.

The results of our tests on previously published clinopyroxene-liquid barometers are summarized in Figure 1. All barometric calculations were performed using experimental temperatures and quoted H_2O

contents where available. Where no H_2O contents were provided, experiments were assumed to be anhydrous. Calculations using data from Villiger et al. (2004, 2007), as well as data from composition 70-002 of Grove et al. (1992), returned extremely variable pressure estimates and were therefore excluded from regressions performed to evaluate the performance of the barometers. We also excluded the results of calculations from a few 1 atm experiments that returned spurious pressures of less than −8 kbar.

Figure 1a shows the performance of model P1 from Putirka et al. (1996), the first formulation of the Jd-in-clinopyroxene barometer (standard error of estimate = 1.4 kbar). Although the test dataset can be fitted reasonably well using a simple linear model (r^2 = 0.81, SEE = 1.1 kbar), the regression does not pass through the origin. Specifically, while the estimates for high pressure (≥7 kbar) experiments lie within one SEE of experimental values (i.e., within 1.4 kbar), estimates for low-pressure experiments are significantly overestimated (intercept = 3.0 kbar), resulting in a mean residual between calculated and experimental pressures of 2.3 kbar. However, given that this model was only calibrated using ≥8 kbar experiments, the poor accuracy at lower pressures is perhaps not surprising.

Figure 1b shows the performance of equation 30 from Putirka (2008), a recalibrated Jd-in-clinopyroxene barometer (calibration SEE = 1.6 kbar) designed for use with evolved and hydrous compositions as well as with primitive and nominally anhydrous compositions (cf., Putirka et al. 2003). Despite being calibrated with a larger and more compositionally diverse dataset, this barometer performed similarly to model P1 from Putirka et al. (1996) in our tests: r^2 = 0.82, SEE = 0.9 kbar, intercept = 3.0 kbar and mean residual = 2.1 kbar. Nevertheless, the low SEE is consistent with the analysis of Putirka (2008) that this is the most precise formulation of the Jd-in-clinopyroxene barometer to date for mafic systems.

Figure 1c shows the performance of equation 32a from Putirka (2008), a barometer that, following the approach of Nimis (1995), is based on temperature and clinopyroxene composition alone (calibration SEE = 3.1 kbar). Although the test data are fitted well by a simple linear model (r^2 = 0.89; SEE = 0.9), pressure

estimates are consistently ~1–2 kbar too high, with the magnitude of the overestimation being greatest at 1 atm (intercept = 2.3 kbar, mean residual 2.0 kbar). We therefore suggest that the systematic overestimation of pressure noted by Putirka (2008) when applying this model to hydrous compositions may extend to H_2O-poor compositions at low to moderate pressures (<10 kbar).

Figure 1d shows the performance of equation 32c from Putirka (2008), a barometer based on Al partitioning between clinopyroxene and liquid (SEE = 1.5 kbar). This barometer performed worst out of the four barometric expressions tested: $r^2 = 0.70$, SEE = 1.5 kbar, intercept = 2.6 kbar and mean residual 1.8 kbar. Despite exploiting Al partitioning instead of Jd formation, this barometer shows a similar pressure-dependent accuracy to the two Jd-in-clinopyroxene barometers shown in Figures 1a and 1b: the barometer is accurate at high pressures (≥7 kbar), but increasingly inaccurate at lower pressures.

A crucial observation from Figure 1 is that pressure overestimation is not restricted to experiments carried out at 1 atm in which Na loss by volatilization may have occurred. Applying Jd-in-clinopyroxene barometers to data from 1–4 kbar experiments carried out in zirconium-hafnium-molybdenum (ZHM) cold seal, IHPV and piston cylinder equipment also results in values 1.5–3.0 kbar above experimental pressures. Pressure overestimations for these closed-capsule experiments cannot be attributed to Na loss from their coexisting liquids, and the cause of the Jd-in-clinopyroxene barometers' spuriously high pressure estimates at low pressures must lie elsewhere. Encouragingly, though, these existing barometers qualitatively, at least, recover the sense of pressure change in the test dataset: taking the mean calculated pressure of the various isobaric datasets, it is possible to place these isobaric sets in the correct order. This indicates that there is merit to the clinopyroxene-liquid approach to barometry, which might be resolved by a suitable recalibration.

METHOD

The performance of a barometer depends strongly on how calibration data are selected. To calibrate a new

clinopyroxene-liquid barometer that is accurate at crustal pressures, it is thus essential to include low- to moderate-pressure experiments (≤7 kbar) in the calibration dataset. Furthermore, given that even small amounts of H_2O can have a strong effect on mineral-liquid equilibria (e.g., Almeev et al. 2007, 2012; Médard et al. 2008), it is also important to include hydrous experiments. A calibration database was thus compiled from the following sources: Blatter and Carmichael (2001), Kinzler and Grove (1992), Moore and Carmichael (1998), Putirka et al. (1996), Sisson and Grove (1993) and Yang et al. (1996). The calibration database contains a total of 113 experiments saturated in clinopyroxene ± olivine ± plagioclase ± orthopyroxene ± spinel ± hornblende ± magnetite ± ilmenite. The inclusion of 1 atm experiments from Yang et al. (1996) represents a key development from the calibration datasets used in previous barometer calibrations. Importantly, this set of 1 atm experiments experienced negligible Na loss. Further details are summarized in Table 1, and the complete dataset is provided in the electronic appendix.

Liquid and clinopyroxene components were calculated following the methods outlined in Tables 1 and 3 from Putirka (2008) respectively. All the clinopyroxene compositions in the calibration dataset return six-oxygen cation sums close to 4 (3.97–4.05), confirming that they are stoichiometric. Linear regression was performed following the procedures outlined in Putirka et al. (1996) and Putirka (2008) to determine the regression coefficients. Following the qualitative success of prior models (Figure 1), the regression equation is based on a thermodynamic description of Jd formation, and includes empirical terms to improve the precision of pressure estimates. The new Jd-in-clinopyroxene barometer has the following form:

$$\mathrm{P(kbar)} = -26.27 + 39.16\frac{\mathrm{T(K)}}{10^4}\ln\left[\frac{X_{Jd}^{cpx}}{X_{NaO_{0.5}}^{liq}X_{AlO_{1.5}}^{liq}\left(X_{SiO_2}^{liq}\right)^2}\right] - 4.22\ln\left(X_{DiHd}^{cpx}\right) + 78.43X_{AlO_{1.5}}^{liq} + 393.81\left(X_{NaO_{0.5}}^{liq}X_{KO_{0.5}}^{liq}\right)^2 \quad (1)$$

This new barometer is calibrated for ultramafic to intermediate compositions in the 0.001–20 kbar and 950–1400 °C ranges. Although this study is focused primarily on H_2O-poor tholeiites, the inclusion of H_2O-rich experiments in the calibration dataset means that the barometer is also suitable for use with hydrous compositions. However, because of Aeg component formation at high fO_2 (Blundy et al. 1995),

281 we advise caution when using this barometer under oxidizing conditions ($fO_2 \geq$ QFM+1); we do not
282 calculate an Fe^{3+} or Aeg component, but pressures may be overestimated if Na is accidentally assigned to
283 Jd when it should be assigned to Aeg. A spreadsheet for calculating pressures is provided in the electronic
284 appendix.
285
286 **RESULTS**
287 Calibration data are fitted well by a simple model (Figure 2a; $r^2 = 0.95$; SEE = 1.3 kbar). Importantly, the
288 accuracy of the new barometer does not vary systematically as a function of pressure (intercept = 0.3
289 kbar); the inaccuracies visible in Figure 1 appear to have been avoided. Given that Jd-in-clinopyroxene
290 barometers depend on temperature as well as composition, they are usually solved iteratively using a
291 complementary thermometric expression, which may itself be pressure dependent. Equation 33 from
292 Putirka (2008) is the most precise clinopyroxene-liquid thermometer currently available (calibration SEE
293 = 45 °C). This thermometer was calibrated using a large global dataset that has minimal overlap with the
294 dataset used to calibrate equation 1. Figure 2b shows pressures estimated for the calibration dataset by
295 solving our new Jd-in-clinopyroxene barometer iteratively with equation 33 from Putirka (2008).
296 Encouragingly, iteratively calculated pressures are very similar to those calculated using experimentally
297 reported temperatures; neither the accuracy not the precision of the pressure estimates suffer from being
298 calculated iteratively ($r^2 = 0.95$; SEE = 1.4 kbar; intercept = 0.6 kbar). Corresponding iteratively
299 calculated temperatures are shown in Figure 2c. Although temperatures appear to be calculated more
300 precisely than the thermometer's quoted uncertainty (SEE = 28 °C versus 45 °C from Putirka, 2008), they
301 are systematically overestimated below 1100 °C. While equation 33 from Putirka (2008) performs well
302 when paired with our new barometer at the temperatures of interest for this study (1100–1300 °C), we
303 advise caution when using this barometer-thermometer combination at low temperatures (≤1100 °C).
304
305 A direct comparison between pressures calculated with the original Jd-in-clinopyroxene calibration from
306 Putirka et al. (1996) and our new calibration is shown in Figure 2d. While the original model reproduces

307 the low pressures of hydrous experiments in the 0.5–2.5 kbar range (Sisson and Grove 1993; Blatter and
308 Carmichael 2001), the 1 atm experiments of Yang et al. (1996) are overestimated by ~4 kbar and do not
309 lie on a regression through the dataset. Comparing Figure 2a with Figure 2d suggests that our new
310 barometer does not suffer from the same inaccuracies at low pressures present in other clinopyroxene-
311 liquid barometers.
312
313 **DISCUSSION**
314 **Evaluating the Jd-in-clinopyroxene Barometer**
315 Although regression statistics from calibration datasets provide important information about the precision
316 of thermobarometric models, it is important to verify model performance with independent datasets that
317 do not contain calibration data. Figure 3 shows the results of tests carried out using a global dataset of
318 clinopyroxene-liquid pairs from experiments conducted above 1 atm and below 20 kbar to avoid the
319 effects of Na loss in legacy datasets while remaining within the barometer's calibration range. This global
320 dataset does not include the data from experiments on H_2O-poor tholeiites used to produce Figure 1, and
321 is provided in the electronic appendix. Clinopyroxene-liquid pairs were also filtered on the basis of being
322 within 20% of $K_{d\,Fe-Mg}^{cpx-liq}$ equilibrium according to equation 35 from Putirka (2008). A total of 624
323 clinopyroxene-liquid pairs fitted these criteria (Bender et al. 1978; Johnston 1986; Kelemen et al. 1990;
324 Meen 1990; Bartels et al. 1991; Vander Auwera and Longhi 1994; Patiño-Douce and Beard 1996; Falloon
325 et al. 1999, 2001, Grove et al. 1997, 2003; Kinzler 1997; Falloon et al. 1997; Gaetani and Grove 1998;
326 Johnson 1998; Kogiso et al. 1998; Robinson et al. 1998; Takahahshi et al. 1998; Vander Auwera et al.
327 1998; Draper and Green 1999; Pickering-Witter and Johnston 2000; Kogiso and Hirschmann 2001;
328 Müntener et al. 2001; Berndt et al. 2001; Schwab and Johnston 2001; Dann et al. 2001; Pichavant et al.
329 2002; Bulatov et al. 2002; Wasylenki et al. 2003; Elkins-Tanton and Grove 2003; Barclay 2004; Laporte
330 et al. 2004; Médard et al. 2004; Parman and Grove 2004; Kägi et al. 2005; Scoates et al. 2006; Di Carlo et
331 al. 2006; Ganino et al. 2013).

Figure 3a shows pressures calculated for the global dataset using imposed experimental temperatures. Although simple linear fits to the global dataset are worse than similar fits to the calibration dataset (r^2 = 0.51; SEE = 3.8 kbar; intercept = 1.5 kbar), the mean residual between experimental and calculated pressures is slightly smaller (−1.3 kbar). Barometer performance was marginally improved when pressures were calculated iteratively (Figure 3b; r^2 = 0.58, SEE = 3.6 kbar; intercept = 0.8 kbar; mean residual = −1.3 kbar). The performance of our new barometer is nonetheless comparable with the performance of previous barometers subjected to testing against global datasets (Putirka 2008). However, the usefulness of performing global tests is somewhat unclear given that many of the experiments in the global dataset were performed on compositions either beyond the range of barometer calibration or of little relevance to the investigation of magmatic processes in the crust. For example, low-pressure (2–4 kbar), high-fO_2 (NNO to NNO+2.3) experiments on phonolitic compositions return pressures ~10 kbar higher than experimental pressures (Figure 3; Berndt et al. 2001). This discrepancy is perhaps unsurprising given that there are no highly alkaline or highly oxidized compositions in the calibration dataset, and may serve as an example of how pressures may be overestimated when Na partitions as Aeg rather than Jd. We therefore carried out a more specific evaluation of barometer performance in basaltic systems using the tholeiitic test dataset used to produce Figure 1. The experiments of Yang et al. (1996) were, however, excluded because they were used in the barometer calibration. Calculations performed on data from Villiger et al. (2004, 2007) and composition 70-002 from Grove et al. (1992) were also excluded because of the large pressure ranges estimated for these experiments.

Figure 4a shows pressures calculated for test data with imposed experimental temperatures and Figure 4b shows pressures for the same data calculated iteratively using equation 33 from Putirka (2008). Figure 4c shows the iteratively calculated temperatures corresponding to Figure 4b. Pressure estimates for the test dataset were determined with similar precisions using both imposed and iteratively calculated temperatures (SEE = 1.1 and 1.2 kbar respectively). Encouragingly, the mean residuals between

experimental and calculated pressures are also small (0.6 and 0.8 kbar respectively). The barometer's ability to reproduce the calibration dataset (SEE = 1.4 kbar; Figure 2b) is a conservative and thus more appropriate estimate of barometer precision for tholeiitic systems.

Regressions through pressures from the test dataset do not pass through the origin as closely as regressions through pressures from the calibration dataset do: intercepts = 1.1 and 1.2 kbar when using imposed and iteratively calculated temperatures respectively. The significance of this inaccuracy is unclear. While the specter of Na loss could still haunt the 1 atm data used here (Toplis and Carroll 1995; Thy et al. 2006), it is important to note that the magnitude of pressure overestimation at 1 atm is indistinguishable from the barometer's inherent uncertainty. This contrasts with the inaccuracies identified in Figure 1, where the pressures of 1 atm experiments are overestimated by more than 2 SEE (~3 kbar). Indeed, our new barometer returns systematically lower pressures for the test dataset than model P1 from Putirka et al. (1996) (Figure 4d). However, improving the precision and accuracy of thermobarometric expressions of the type we present here is challenging for two reasons. Firstly, both the calibration and application of Jd-in-clinopyroxene barometers are strongly affected by the ability to measure Na_2O in glasses and clinopyroxenes by electron probe precisely: Na_2O can be mobile under electron beams and is often present at only 0.1–0.5 wt.% levels in clinopyroxenes. Secondly, barometry using condensed phases (i.e., solids and liquids) is limited by the small absolute magnitudes of partial molar volume changes associated with reactions that can be exploited as barometers, i.e., a precision of 1.4 kbar may be close to the limit of what can be achieved using current approaches (Putirka 2016).

Magma Storage Pressures under Icelandic Rift Zones

Selecting Appropriate Clinopyroxene Analyses. Magma storage pressures have been estimated using the products of a number of tholeiitic eruptions from Iceland's neovolcanic rift zones using Jd-in-clinopyroxene barometry (Maclennan et al. 2001; Winpenny and Maclennan 2011; Hartley and Thordarson 2013; Neave et al. 2013, 2015; Geiger et al. 2016). However, most studies followed different

methodologies, making inter-eruption comparisons unreliable. For example, different studies used different barometers and different methods of selecting equilibrium clinopyroxene-liquid pairs, and while some studies applied empirical corrections to account for the systematic errors highlighted in Figure 1, others did not. In order to investigate magma storage pressures of Icelandic tholeiites systematically, we compiled clinopyroxene data from the highly primitive Borgarhraun lava ($Mg\#_{liq}$ ~69, assuming $Fe^{3+}/\Sigma Fe$ = 0.85, Shorttle et al. 2015), the moderately primitive Thjórsá and Skuggafjöll flows ($Mg\#_{liq}$ ~50–54) and the evolved Laki flow and 10 ka Grímsvötn tephra series ($Mg\#_{liq}$ ~45). We also included data from the moderately primitive Holuhraun 1 and 2 eruptions ($Mg\#_{liq}$ ~50) that took place at the same location as the 2014–2015 eruption in 797 and 1862–1864 (Hartley and Thordarson 2013). Data sources are listed in Table 2.

Compiled Icelandic clinopyroxene compositions are summarized in Figure 5 using components calculated according to the methods outlined in Table 3 from Putirka (2008). Individual eruptions form distinct arrays in both DiHd-EnFs space and DiHd-CaTs space (Figures 5a and 5b). While some eruptions form single arrays in Ca/(Ca+Mg+Fe)-Al space, others form multiple arrays (Figure 5c). Eruptions also form single arrays in Ca/(Ca+Mg+Fe)-Jd space (Figure 5d). The large compositional ranges in Figure 5 represent not only the pressure and temperature conditions at which the crystals formed, but also analytical errors, the occurrence of sector zoning and the diversity of primary melt compositions supplied to Icelandic magmatic systems. To calculate storage pressures robustly, the effects of these three factors on barometric calculations must be considered.

Analytical errors can strongly affect the results of thermobarometric calculations. We therefore applied two filters to screen our dataset for poor analyses before performing any calculations. Firstly, we excluded all clinopyroxene compositions that returned non-stoichiometric values when cation sums were calculated on a six-oxygen basis (6O). Specifically, analyses with 6O sums of <3.99 or >4.02 were discarded. Secondly, we excluded all analyses with Jd < 0.01, which represent Na_2O contents at or below the

detection limit of EPMA. The few analyses with Jd contents below 0.01 lie away from the bulk of the data from their respective eruptions, confirming the poor quality of these analyses.

Sector zoning resulting from the variable partitioning of certain elements onto different crystal faces during growth is extremely common in igneous clinopyroxenes (Strong 1969; Nakamura 1973; Downes 1974). The rate of crystal growth, itself closely related to the degree of undercooling (ΔT), exerts a first order control on the style of sector zoning (Kouchi et al. 1983). For example, at high degrees of undercooling (ΔT ~−45 °C), pressure-sensitive Na and Al partition onto {−111} faces of clinopyroxene crystal that record compositions strongly out of equilibrium (Welsch et al. 2016). In contrast, at low degrees of undercooling (ΔT ~−20 °C), the sense of partitioning can be reversed, with Al partitioning variably onto {100}, {010} and {110} faces depending on the exact conditions experienced. Clinopyroxenes from tholeiitic systems often display strong sector zoning in their Ca/(Ca+Mg+Fe) contents, which results from the disequilibrium partitioning of Mg and Fe onto {100} faces causing concurrent dilutions of Ca and Al (Nakamura 1973). Before performing thermobarometric calculations it is thus essential to evaluate which sector zones were closest to being in equilibrium at the time of crystallization (Hammer et al. 2016). For example, low-Al zones in high-Al clinopyroxenes from the Haleakala ankaramite, Hawai'i, which crystallized at high degrees of undercooling, record the compositions closest to being in equilibrium at the time of formation (Hammer et al. 2016; Welsch et al. 2016).

In the Icelandic clinopyroxene populations where it is present, sector zoning is clearly resolved in Ca/(Ca+Mg+Fe)-Al space (Figure 5c): one set of sectors defines a high-Al field with high-Ca/(Ca+Mg+Fe) while the other defines a low-Al field with variable-Ca/(Ca+Mg+Fe). This type of sector zoning is common in clinopyroxenes formed at low degrees of undercooling in tholeiitic magmas (Nakamura 1973). Following Nakamura (1973), we conclude that the low-Al sectors experienced Ca and Al dilution during growth as a result of the disequilibrium incorporation of Mg and Fe, and that the high-

Al sectors preserve the compositions that were closest to equilibrium during their near-isothermal crystallization (Neave et al. 2013). We therefore applied a third filter to our clinopyroxene dataset before carrying out thermobarometry: all compositions with Al (6O) < 0.11 were excluded (Figure 5c). Furthermore, almost all un-zoned clinopyroxenes from a series of recent equilibrium crystallization experiments carried out on tholeiitic starting compositions at a range of pressures (1–7 kbar) have Al (6O) > 0.11 (Husen et al. 2016), confirming that high-Al zones preserve the best record of clinopyroxene-liquid equilibrium at the time of crystallization in the samples considered here. It is nonetheless important to note that diffusive pile-up during crystallization at high degrees of undercooling can result in Al, Na and Ti enrichments that compromise the identification of near-equilibrium zones (Mollo et al. 2013b).

Performing Thermobarometric Calculations. The selection of appropriate equilibrium liquids is a pre-eminent consideration when calculating storage pressures by Jd-in-clinopyroxene barometry. In some cases, textural relationships between crystals and their carrier liquids (i.e., matrix glasses) indicate that these two phases were in equilibrium at the time of quenching and can be used for thermobarometric calculations. However, many clinopyroxenes are concentrically zoned, reflecting growth in different magmatic environments because of magma mixing and fractionation crystallization prior to eruption. Indeed, many instances of crystal-liquid disequilibrium have been described in Icelandic tholeiites (e.g., Hansen and Grönvold 2000; Halldórsson et al. 2008; Thomson and Maclennan 2013; Neave et al. 2014), demonstrating that equilibrium clinopyroxene-liquid pairs must be selected with care.

Kernel density estimates (KDEs) of $Mg\#_{cpx}$ values calculated with a bandwidth corresponding to the 1σ precision of $Mg\#_{cpx}$ determination (±0.5 mol.%) are shown in Figure 6a (Rudge 2008; Thomson and Maclennan 2013). The compositions of clinopyroxene crystals predicted to be in equilibrium with the average carrier liquid compositions from each eruption are shown as vertical bars in Figure 6a. These compositions were calculated using $K_{d\,Fe-Mg}^{cpx-liq}$ values from equation 35 from Putirka (2008), liquid

461 $Fe^{3+}/\Sigma Fe$ values of 0.85, temperatures from equation 15 from Putirka (2008) and matrix glass
462 compositions collated from the following sources: Holuhraun 1 and 2, Hartley and Thordarson (2013);
463 Laki, Hartley et al. (2014); 10 ka Grímsvötn tephra series, Neave et al. (2015), Skuggafjöll, Neave et al.
464 (2014); and Borgarhraun Sigurdsson et al. (2000). No matrix glasses are known from the crystalline
465 Thjórsá lava, so the average composition of groundmass separates, which may have experienced olivine
466 and clinopyroxene accumulation, was used instead (Halldórsson et al. 2008). Hence, the equilibrium
467 $Mg\#_{cpx}$ value calculated for the Thjórsá carrier liquid was probably overestimated. Figure 6a reveals that
468 the majority of clinopyroxene compositions in our compilation crystallized from liquids significantly
469 more primitive than those which carried them to the surface, mirroring similar observations from olivine
470 and plagioclase populations (Hansen and Grönvold 2000; Thomson and Maclennan 2013). Therefore,
471 matrix glass compositions are not plausible equilibrium liquids for most of the analyses in our
472 compilation of Icelandic clinopyroxenes.
473
474 In order to increase the number of available clinopyroxene-liquid pairs and hence estimate the storage
475 pressures of primitive clinopyroxenes, we used an iterative equilibrium liquid-matching algorithm similar
476 to those used by Winpenny and Maclennan (2011) and Neave et al. (2013, 2015). Putative equilibrium
477 liquids were selected from a large database of Icelandic whole-rock and matrix glass compositions
478 collated by Shorttle and Maclennan (2011), to which further additions have been made from more recent
479 studies (Jude-Eton et al. 2012; Koornneef et al. 2012; Hartley and Thordarson 2013; Hartley et al. 2014;
480 Neave et al. 2014, 2015; Streeter and Dugmore 2014). To avoid selecting geologically implausible alkali
481 basalt compositions, all data from flank zone eruptions were excluded. Furthermore, highly primitive
482 compositions (MgO > 12 wt.%) liable to be affected by olivine accumulation were also excluded from the
483 database.
484
485 In the first iteration of the liquid-matching algorithm, equilibrium melts were selected on the basis of
486 being within 20% of Fe-Mg equilibrium with each clinopyroxene analysis according to the temperature-

487 independent model of Wood and Blundy (1997). Initial guesses for equilibrium pressures and
488 temperatures were then calculated for every successfully matched clinopyroxene-liquid pair by iteratively
489 solving our new Jd-in-clinopyroxene barometer with equation 33 from Putirka (2008). Pressures and
490 temperatures were subsequently refined by performing several further iterations of this procedure with
491 more stringent criteria for selecting equilibrium melts (cf., Mollo et al. 2013a). Specifically,
492 clinopyroxene-liquid pairs were selected on the basis of being within 10% of Fe-Mg, DiHd component,
493 CaTs component and Ti equilibrium according to equation 35 from Putirka (2008), the DiHd and CaTs
494 equilibrium models from Putirka (1999) and the Ti partitioning model from Hill et al. (2011) respectively.
495 The inclusion of criteria for Ti and CaTs component equilibrium is important to account for the effects of
496 mantle-derived variability in liquid compositions (Shorttle and Maclennan 2011). Median pressures and
497 temperatures for each clinopyroxene analysis were calculated at the end of each iteration for use as
498 starting guesses in the next iteration.
499
500 **Interpreting the Results of Thermobarometric Calculations.** Out of the initial compilation of 1037
501 clinopyroxene analyses, a total of 603 were successfully matched to between 1 and 1167 glass and whole-
502 rock compositions (median = 184 matches). $Mg\#_{cpx}$ values to which equilibrium liquids were successfully
503 matched are summarized in Figure 6b. Although sufficient matches were made to estimate magma storage
504 pressures for each eruption, no matches were found for some ranges of clinopyroxene composition. For
505 example, no matches were found for the most primitive clinopyroxene analyses from the Borgarhraun
506 lava. In the cases of the Laki and Thjórsá lavas, and the 10 ka Grímsvötn tephra series, matched $Mg\#_{cpx}$
507 values have bimodal distributions. Given that this bimodality represents the crystallization of different
508 crystal populations under different conditions (Halldórsson et al. 2008; Neave et al. 2013, 2015), storage
509 pressure estimates for the evolved and primitive populations were considered independently. The
510 compositions of successfully matched clinopyroxene analyses are summarized in Figure 7 and form much
511 tighter clusters than the input data shown in Figure 5.
512

Iteratively calculated pressures and temperatures are summarized in Figure 8 and provided in the electronic appendix. The full dataset of clinopyroxene-liquid pairs is available from the corresponding author on request. As expected, there is an appreciable positive correlation between $Mg\#_{cpx}$ and equilibrium temperature (r^2 = 0.64; Figure 8a). There is no strong relationship between $Mg\#_{cpx}$ and equilibrium pressure, with the exception of high-Mg# clinopyroxenes from the Borgarhraun lava returning higher pressures (r^2 = 0.29 with Borgarhraun, but 0.13 without; Figure 8b). Conversely, while there is probably no relationship between clinopyroxene Al (6O) and temperature (r^2 = 0.14; Figure 8c), there may be a very weak positive correlation between Al (6O) and pressure (r^2 = 0.2; Figure 8d).

In some cases, large ranges of pressures calculated for individual clinopyroxene populations have been interpreted as evidence for vertically extensive magma storage regions (e.g., Budd et al. 2016; Giacomoni et al. 2016). However, the certainty with which pressures can be calculated using clinopyroxene-liquid barometers is limited (Figures 1–4). For example, the new Jd-in-clinopyroxene calibration presented here has an SEE of 1.4 kbar, indicating that only 67% of the calibration data lie within 1.4 kbar of a regression through the calibration dataset. In order to test whether the large pressure ranges observed in Figure 8 represent polybaric storage or merely the inherent uncertainty of the barometric calculations, data were converted to KDEs that were in turn fitted with Gaussian functions (Figure 9; Rudge 2008). KDEs were calculated with an imposed bandwidth of 1.4 kbar, which is equivalent to the estimated SEE of the barometer calibration. Gaussian functions fitted to pressure KDEs calculated for each clinopyroxene population identified in Figure 6b have standard deviations of 1.5–1.8 kbar that are only slightly larger than the SEE of the barometer itself (Table 3). The SEEs of pressures calculated for each clinopyroxene population, which may be better estimates of precision than standard deviations in such datasets (e.g., Putirka 2016), are also substantially smaller than the SEE of the barometer (0.1–0.4 kbar versus 1.4 kbar; Table 3). Thus, the variability in the pressures calculated for individual clinopyroxene populations feasibly reflects uncertainties in either the barometric model or the equilibrium liquid-matching procedure rather than crystallization over a large pressure range. In other words, while different clinopyroxene

539 populations may have crystallized at different pressures, individual populations are likely to have
540 crystallized within a narrow pressure window of 0.1–0.4 kbar.
541
542 The means of Gaussian fits to the results of thermobarometric calculations represent our best magma
543 storage pressure estimates (Table 3). The highest storage pressures were calculated for the highly
544 primitive ($Mg\#_{cpx}$ > 85) Borgarhraun lava (4.8±1.8(1σ) kbar). However, these values are significantly
545 lower than previous estimates (8.1±1.1(1σ) kbar; Maclennan et al. 2012; Winpenny and Maclennan 2011).
546 We identify two possible reasons for this discrepancy: firstly, we obtained few matches to the most
547 primitive clinopyroxenes ($Mg\#_{cpx}$ > 90) that are most likely to have crystallized at high pressures; and
548 secondly, although the Putirka et al. (1996) barometer used by Winpenny and Maclennan (2011)
549 performed best at 8–10 kbar when tested with experimental data (Figure 1a), it appears to converge
550 towards high pressures when performing iterative calculations on natural data (Supplementary Figure 1).
551 Assuming an average Icelandic crustal density of 2.86 $Mg.m^{-3}$ (Carlson and Herrick 1990), a storage
552 pressure of 4.8±1.8(1σ) kbar corresponds to lower crustal depths of 13.7±5.1(1σ) km (Moho depth ~20
553 km; Darbyshire et al. 2000).
554
555 Moderately primitive clinopyroxenes ($Mg\#_{cpx}$ ~80–86) in the Laki, Thjórsá and Skuggafjöll lavas, and the
556 10 ka Grímsvötn tephra series from the EVZ returned very similar mean pressures of 3.5–3.7 kbar with
557 1σ uncertainties of 1.5–1.8 kbar. These values are broadly consistent with previous estimates of 2–5.4
558 kbar and 2.5–5.5 kbar for the Laki lava and 10 ka Grímsvötn tephra series calculated by applying
559 empirical corrections to published barometers (Neave et al. 2013, 2015). Pressures of 3.5–3.7 kbar
560 correspond to mid-crustal depths of 10.0–10.6±4.3–5.1(1σ) km (Moho depth ~25–35 km; Darbyshire et
561 al. 2000). More evolved clinopyroxenes ($Mg\#_{cpx}$ < 80) from the same samples of the Laki and Thjórsá
562 lavas and the 10 ka Grímsvötn tephra series returned slightly lower pressures of 2.5–2.8±1.5–1.7(1σ)
563 kbar, which corresponds to depths of 7.2–8.0±4.3–4.9(1σ) km. The ~1 kbar difference in mean storage
564 pressures between primitive and evolved clinopyroxene populations suggests that crystallization may

565 have occurred at different depths. Indeed, pressures of final equilibration based on OPAM barometry
566 suggest that the evolved assemblage crystallized at low pressures (1–2±1 kbar), though a low-pressure
567 overprint could have been imposed during final ascent (Neave et al. 2013, 2015).
568
569 Moderately primitive clinopyroxenes ($Mg\#_{cpx}$ ~80) from the Holuhraun 1 and 2 lavas returned the lowest
570 storage pressures of 2.4±1.7(1σ) kbar, which are substantially lower than previously reported values (2.3–
571 7.6 kbar; Hartley and Thordarson 2013). The pressures we calculated from the Holuhraun 1 and 2 lavas
572 are also substantially lower than recent estimates from the petrologically analogous 2014–2015
573 Holuhraun lava (4.7 kbar; Geiger et al. 2016). These discrepancies probably reflect the inaccuracies in
574 previously published barometers (e.g., Supplementary Figure 1). Interestingly, a pressure of 2.4±1.7(1σ)
575 kbar translates to a depth of 6.9±4.9(1σ) km, which corresponds closely to the depth of dyke
576 emplacement during the 2014–2015 eruption (5–7 km; Ágústsdóttir et al. 2015) as well as to geodetically
577 inferred magma storage depths under the Bárðarbunga caldera (8–12 km; Gudmundsson et al. 2016).
578

579 ## IMPLICATIONS

580 ### The Accuracy and Precision of Jd-in-clinopyroxene Barometry

581 Tests performed on a range of clinopyroxene-liquid barometers reveal that currently published models
582 routinely overestimate the pressure of experimental clinopyroxene-liquid pairs at crustal storage
583 conditions, i.e., ≤7 kbar. The accuracy of current Jd-in-clinopyroxene barometers is pressure dependent,
584 with overestimates being greatest at 1 atm. Although these tests were designed to investigate the accuracy
585 and precision of barometers at the conditions relevant to magma evolution under Iceland's rift zones (i.e.,
586 the storage of low-H_2O tholeiitic basalts), they demonstrate the importance of evaluating barometer
587 performance at the conditions of interest before interpreting any results (e.g., Masotta et al. 2013).
588 Therefore, numerous storage pressures calculated using clinopyroxene-liquid barometers may have been
589 overestimated by up to 3 kbar, and pressure estimates from MORB and OIB settings are likely to have
590 been affected with the greatest certainty. It may thus be necessary to reassess a number of published

591 magma storage pressure estimates, particularly in situations where they are used to inform monitoring
592 strategies in volcanically active regions.
593
594 Our new Jd-in-clinopyroxene barometer offers a significant improvement in accuracy over previous
595 versions of the barometer: calibration data are reproduced with a high degree of accuracy and testing
596 against a global dataset reveals a maximum overestimation of 1.5 kbar at 1 atm; testing against
597 experiments on H_2O-poor tholeiites reveals a lower maximum overestimation of 1.2 kbar at 1 atm.
598 Although our new calibration is a substantial improvement on its forebears, it should nevertheless be
599 tested further as experimental databases continue to expand. The new barometer's precision (SEE = 1.4
600 kbar) is probably close to the limit of what can be achieved with the Jd-liquid reaction. It is thus essential
601 to consider the inherent imprecision of Jd-in-clinopyroxene barometers when interpreting calculation
602 results. For example, pressure distributions calculated from multiple analyses that approximate Gaussian
603 bell curves with standard deviations of ~1.4 kbar may only reflect model uncertainties rather than
604 polybaric distributions of magma storage. New approaches, such as integrating numerous mineral-mineral
605 and mineral-liquid thermobarometric equations, as is commonly undertaken in thermobarometric studies
606 of metamorphic rocks (Powell and Holland 2008), will probably be necessary to improve the barometric
607 precision in magmatic systems.
608
609 **Magma Storage Pressures under Iceland's Neovolcanic Rift Zones**
610 Our calculations provide an internally consistent insight into the storage pressures of a range of Icelandic
611 rift zone tholeiites. In line with previous observations, high-Mg# clinopyroxenes from the Borgarhraun
612 lava record the highest pressures in our dataset (4.8±1.8(1σ) kbar; 13.7±5.1(1σ) km), suggesting that near-
613 primary melts undergo substantial processing in the lower crust prior to eruption or intrusion to shallower
614 levels (Winpenny and Maclennan 2011). Indeed, patterns of microseismicity under the NVZ provide
615 strong evidence for the formation of intrusions in the lower crust (Hooper et al. 2011; Greenfield and
616 White 2015), where much of the initial compositional variability of primary mantle melts is probably

617 destroyed by mixing (Maclennan 2008). However, the discrepancy between the pressures calculated here
618 (4.8±1.8(1σ) kbar) and those reported previously (8.1±1.1(1σ) kbar) should be noted (Winpenny and
619 Maclennan 2011). Further experiments on primitive basalts should help to elucidate the causes of this
620 inconsistency, though an inability to identify equilibrium melts for highly primitive clinopyroxenes may
621 have also biased our calculations towards lower pressures. A storage pressure of 4.8±1.8(1σ) kbar thus
622 represents a robust minimum value for the Borgarhraun magma.
623
624 Most of the eruption products we considered show evidence for crystallization in the Icelandic mid-crust.
625 Those containing compositionally bimodal clinopyroxene populations suggest that crystallization may
626 have occurred at two pressure intervals, 3.5–3.7±1.5–1.8(1σ) kbar and 2.5–2.8±1.5–1.7(1σ) kbar.
627 However, given the large inherent uncertainties in Jd-in-clinopyroxene pressure estimates, it is currently
628 unclear whether these different pressures genuinely reflect polybaric crystallization. Nevertheless, the
629 conclusion that Icelandic rift zone tholeiites are primarily stored and processed in the mid-crust (2.5–3.7
630 kbar; 7.2–10.6 km) is robust. While a depth range of 7.2–10.6 km overlaps with some geodetic and
631 geophysical estimates of magma storage depths under Icelandic rift zones (Reverso et al. 2014;
632 Guðmundsson et al. 2016), many estimates from central volcanoes are significantly shallower (2–4 km;
633 Alfaro et al. 2007; de Zeeuw-van Dalfsen et al. 2012; Hreinsdóttir et al. 2014). However, with the
634 possible exception of the 10 ka Grímsvötn tephra series, none of the volcanic products we considered
635 were erupted from central volcanoes, indicating that they probably bypassed shallow storage zones *en*
636 *route* to the surface, as occurs in Hawai'i (Poland 2015).
637
638 Although our calculations compress the pressure ranges reported by previous studies using the same
639 clinopyroxene analyses (e.g., 2.8–3.8 kbar for Laki in contrast with 2.0–5.4 kbar; Neave et al. 2013),
640 integrating results across multiple eruptions and clinopyroxene populations indicates that magma storage
641 occurs across a range of depths under Icelandic rift zones (at least 2.5–4.8 kbar). Thus, accretion of the
642 Icelandic crust ostensibly proceeds in a similar manner to that outlined by stacked sill-type models from

643 mid-ocean ridges (Boudier et al. 1996; Kelemen et al. 1997; Maclennan et al. 2001).

644

645 **ACKNOWLEDGEMENTS**

646 We thank Silvio Mollo and one anonymous reviewer for their helpful and constructive reviews, as well as
647 Georg Zellmer for his efficient editorial handling. DAN acknowledges support from the Alexander von
648 Humboldt Foundation.

649

650 **REFERENCES CITED**

651 Ágústsdóttir, T., Woods, J., Greenfield, T., Green, R.G., White, R.S., Brandsdóttir, B., Steinthorsson, S.,
652 and Soosalu, H. (2015) Episodic propagation of the 2014 Bárðarbunga-Holuhraun dike intrusion,
653 central Iceland. Geophysical Research Letters, 43, 9.
654 Alfaro, R., Brandsdóttir, B., Rowlands, D.P., White, R.S., and Guðmundsson, M.T. (2007) Structure of the
655 Grímsvötn central volcano under the Vatnajökull icecap, Iceland. Geophysical Journal International,
656 168, 863–876.
657 Almeev, R.R., Holtz, F., Koepke, J., Parat, F., and Botcharnikov, R.E. (2007) The effect of H_2O on olivine
658 crystallization in MORB: Experimental calibration at 200 MPa. American Mineralogist, 92, 670–
659 674.
660 Almeev, R.R., Holtz, F., Koepke, J., and Parat, F. (2012) Experimental calibration of the effect of H_2O on
661 plagioclase crystallization in basaltic melt at 200 MPa. American Mineralogist, 97, 1234–1240.
662 Annen, C., Blundy, J.D., and Sparks, R.S.J. (2006) The genesis of intermediate and silicic magmas in
663 deep crustal hot zones. Journal of Petrology, 47, 505–539.
664 Barclay, J. (2004) A hornblende basalt from western Mexico: Water-saturated phase relations constrain a
665 pressure-temperature window of eruptibility. Journal of Petrology, 45, 485–506.
666 Bartels, K.S., Kinzler, R.J., and Grove, T.L. (1991) High pressure phase relations of primitive high-
667 alumina basalts from Medicine Lake volcano, northern California. Contributions to Mineralogy and
668 Petrology, 108, 253–270.

669 Bender, J.F., Hodges, F.N., and Bence, A.E. (1978) Petrogenesis of basalts from the project FAMOUS
670 area: experimental study from 0 to 15 kbars. Earth and Planetary Science Letters, 41, 277–302.
671 Berndt, J., Holtz, F., and Koepke, J. (2001) Experimental constraints on storage conditions in the
672 chemically zoned phonolitic magma chamber of the Laacher See volcano. Contributions to
673 Mineralogy and Petrology, 140, 469–486.
674 Berndt, J., Liebske, C., Holtz, F., Freise, M., Nowak, M., Ziegenbein, D., Hurkuck, W., and Koepke, J.
675 (2002) A combined rapid-quench and H_2-membrane setup for internally heated pressure vessels:
676 Description and application for water solubility in basaltic melts. American Mineralogist, 87, 1717–
677 1726.
678 Berndt, J., Koepke, J., and Holtz, F. (2005) An experimental investigation of the influence of water and
679 oxygen fugacity on differentiation of MORB at 200 MPa. Journal of Petrology, 46, 135–167.
680 Blatter, D.L., and Carmichael, I.S.E. (2001) Hydrous phase equilibria of a Mexican high-silica andesite: A
681 candidate for a mantle origin? Geochimica et Cosmochimica Acta, 65, 4043–4065.
682 Blundy, J.D., and Cashman, K. V. (2008) Petrologic reconstruction of magmatic system variables and
683 processes. Reviews in Mineralogy and Geochemistry, 69, 179–239.
684 Blundy, J.D., Falloon, T.J., Wood, B.J., and Dalton, J.A. (1995) Sodium partitioning between
685 clinopyroxene and silicate melts. Journal of Geophysical Research: Solid Earth, 100, 15501–15515.
686 Botcharnikov, R.E., Almeev, R.R., Koepke, J., and Holtz, F. (2008) Phase relations and liquid lines of
687 descent in hydrous ferrobasalt – Implications for the Skaergaard intrusion and Columbia River flood
688 basalts. Journal of Petrology, 49, 1687–1727.
689 Boudier, F., Nicolas, A., and Ildefonse, B. (1996) Magma chambers in the Oman ophiolite: fed from the
690 top and the bottom. Earth and Planetary Science Letters, 144, 239–250.
691 Bucholz, C.E., Gaetani, G.A., Behn, M.D., and Shimizu, N. (2013) Post-entrapment modification of
692 volatiles and oxygen fugacity in olivine-hosted melt inclusions. Earth and Planetary Science Letters,
693 374, 145–155.
694 Budd, D.A., Troll, V.R., Dahren, B., and Burchardt, S. (2016) Persistent two-tiered magma plumbing

beneath Katla volcano, Iceland. Geochemistry, Geophysics, Geosystems, 17, 966–980.

Bulatov, V.K., Girnis, A. V., and Brey, G.P. (2002) Experimental melting of a modally heterogeneous mantle. Mineralogy and Petrology, 75, 131–152.

Carlson, R.L., and Herrick, C.N. (1990) Densities and porosities in the oceanic crust and their variations with depth and age. Journal of Geophysical Research, 95, 9153–9170.

Cashman, K. V., and Sparks, R.S.J. (2013) How volcanoes work: A 25 year perspective. Bulletin of the Geological Society of America, 125, 664–690.

Chatterjee, N., Bhattacharji, S., and Fein, C. (2005) Depth of alkalic magma reservoirs below Kolekole cinder cone, Southwest rift zone, East Maui, Hawaii. Journal of Volcanology and Geothermal Research, 145, 1–22.

Cottrell, E., and Kelley, K.A. (2011) The oxidation state of Fe in MORB glasses and the oxygen fugacity of the upper mantle. Earth and Planetary Science Letters, 305, 270–282.

Dann, J.C., Holzheid, A.H., Grove, T.L., and McSween, H.Y. (2001) Phase equilibria of the Shergotty meteorite: Constraints on pre-eruptive water contents of martian magmas and fractional crystallization under hydrous conditions. Meteoritics & Planetary Science, 36, 793–806.

Darbyshire, F.A., White, R.S., and Priestley, K.F. (2000) Structure of the crust and uppermost mantle of Iceland from a combined seismic and gravity study. Earth and Planetary Science Letters, 181, 409–428.

de Zeeuw-van Dalfsen, E., Pedersen, R., Hooper, A., and Sigmundsson, F. (2012) Subsidence of Askja caldera 2000–2009: Modelling of deformation processes at an extensional plate boundary, constrained by time series InSAR analysis. Journal of Volcanology and Geothermal Research, 213–214, 72–82.

Di Carlo, I., Pichavant, M., Rotolo, S.G., and Scaillet, B. (2006) Experimental crystallization of a high-K arc basalt: The golden pumice, Stromboli volcano (Italy). Journal of Petrology, 47, 1317–1343.

Dixon, J.E., and Stolper, E.M. (1995) An experimental study of water and carbon dioxide solubilities in mid-ocean ridge basaltic liquids. Part I: Calibration and Solubility Models. Journal of Petrology, 36,

721 1633–1646.
722 Downes, M.J. (1974) Sector and oscillatory zoning in calcic augites from M. Etna, Sicily. Contributions
723 to Mineralogy and Petrology, 47, 187–196.
724 Draper, D.S., and Green, T.H. (1999) P-T phase relations of silicic, alkaline, aluminous liquids: New
725 results and applications to mantle melting and metasomatism. Earth and Planetary Science Letters,
726 170, 255–268.
727 Edmonds, M. (2008) New geochemical insights into volcanic degassing. Philosophical Transactions of
728 the Royal Society A: Mathematical, Physical and Engineering Sciences, 366, 4559–4579.
729 Elkins-Tanton, L.T., and Grove, T.L. (2003) Evidence for deep melting of hydrous metasomatized mantle:
730 Pliocene high-potassium magmas from the Sierra Nevadas. Journal of Geophysical Research, 108,
731 2350.
732 Falloon, T.J., Green, D.H., O'Neill, H.S.C., and Hibberson, W.O. (1997) Experimental tests of low degree
733 peridotite partial melt compositions: implications for the nature of anhydrous near-solidus peridotite
734 melts at 1 GPa. Earth and Planetary Science Letters, 152, 149–162.
735 Falloon, T.J., Green, D.H., Danyushevsky, L. V., and Faul, U.H. (1999) Peridotite Melting at 1.0 and 1.5
736 GPa: An Experimental Evaluation of Techniques using Diamond Aggregates and Mineral Mixes for
737 Determination of Near-solidus Melts. Journal of Petrology, 40, 1343–1375.
738 Falloon, T.J., Danyushevsky, L. V., and Green, D.H. (2001) Peridotite Melting at 1 GPa: Reversal
739 Experiments on Partial Melt Compositions Produced by Peridotite–Basalt Sandwich Experiments.
740 Journal of Petrology, 42, 2363–2390.
741 Gaetani, G.A., and Grove, T.L. (1998) The influence of water on melting of mantle peridotite.
742 Contributions to Mineralogy and Petrology, 131, 323–346.
743 Ganino, C., Arndt, N.T., Chauvel, C., Jean, A., and Athurion, C. (2013) Melting of carbonate wall rocks
744 and formation of the heterogeneous aureole of the Panzhihua intrusion, China. Geoscience Frontiers,
745 4, 535–546.
746 Geiger, H., Mattsson, T., Deegan, F.M., Troll, V.R., Burchardt, S., Gudmundsson, Ó., Tryggvason, A.,

747 Krumbholz, M., and Harris, C. (2016) Magma plumbing for the 2014-2015 Holuhraun eruption,
748 Iceland. Geochemistry, Geophysics, Geosystems, 17, 1–16.
749 Giacomoni, P.P., Coltorti, M., Bryce, J.G., Fahnestock, M.F., and Guitreau, M. (2016) Mt. Etna plumbing
750 system revealed by combined textural, compositional, and thermobarometric studies in
751 clinopyroxenes. Contributions to Mineralogy and Petrology, 171, 34.
752 Greenfield, T., and White, R.S. (2015) Building icelandic igneous crust by repeated melt injections.
753 Journal of Geophysical Research: Solid Earth, 120, 7771–7788.
754 Grove, T.L., Kinzler, R.J., and Bryan, W.B. (1992) Fractionation of Mid-Ocean Ridge Basalt (MORB).
755 Mantle Flow and Melt Generation at Mid-Ocean Ridges, Geophysical Monograph 71, American
756 Geophysical Union, 281–310.
757 Grove, T.L., Donnelly-Nolan, J.M., and Housh, T. (1997) Magmatic processes that generated the rhyolite
758 of Glass Mountain, Medicine Lake volcano, N. California. Contributions to Mineralogy and
759 Petrology, 127, 205–223.
760 Grove, T.L., Elkins-Tanton, . T., Parman, S.W., Chatterjee, N., Müntener, O., and Gaetani, G.A. (2003)
761 Fractional crystallization and mantle-melting controls on calc-alkaline differentiation trends.
762 Contributions to Mineralogy and Petrology, 145, 515–533.
763 Guðmundsson, M.T., Jónsdóttir, K., Hooper, A., Holohan, E.P., Halldórsson, S.A., Ófeigsson, B.G.,
764 Cesca, S., Vogfjörd, K.S., Sigmundsson, F., Högnadóttir, T., and others (2016) Gradual caldera
765 collapse at Bárdarbunga volcano, Iceland, regulated by lateral magma outflow. Science, 353.
766 Halldórsson, S.A., Óskarsson, N., Sigurdsson, G., Sverrisdottir, G., and Steinthórsson, S. (2008) Isotopic-
767 heterogeneity of the Thjorsa lava-Implications for mantle sources and crustal processes within the
768 Eastern Rift Zone, Iceland. Chemical Geology, 255, 305–316.
769 Hammer, J.E., Jacob, S., Welsch, B., Hellebrand, E., and Sinton, J.M. (2016) Clinopyroxene in postshield
770 Haleakala ankaramite 1. Efficacy of thermobarometry. Contributions to Mineralogy and Petrology.
771 Hansen, H., and Grönvold, K. (2000) Plagioclase ultraphyric basalts in Iceland: The mush of the rift.
772 Journal of Volcanology and Geothermal Research, 98, 1–32.

773 Hansteen, T.H., and Klügel, A. (2008) Fluid Inclusion Thermobarometry as a Tracer for Magmatic
774 Processes. Reviews in Mineralogy and Geochemistry, 69, 143–177.
775 Hansteen, T.H., Klügel, A., and Schmincke, H.-U. (1998) Multi-stage magma ascent beneath the Canary
776 Islands: evidence from fluid inclusions. Contributions to Mineralogy and Petrology, 132, 48–64.
777 Hartley, M.E., and Thordarson, T. (2013) The 1874-1876 volcano-tectonic episode at Askja, North
778 Iceland: Lateral flow revisited. Geochemistry, Geophysics, Geosystems, 14, 2286–2309.
779 Hartley, M.E., Maclennan, J., Edmonds, M., and Thordarson, T. (2014) Reconstructing the deep CO_2
780 degassing behaviour of large basaltic fissure eruptions. Earth and Planetary Science Letters, 393,
781 120–131.
782 Henstock, T.J., Woods, A.W., and White, R.S. (1993) The accretion of oceanic crust by episodic sill
783 intrusion. Journal of Geophysical Research, 98, 4143.
784 Hill, E., Blundy, J.D., and Wood, B.J. (2011) Clinopyroxene-melt trace element partitioning and the
785 development of a predictive model for HFSE and Sc. Contributions to Mineralogy and Petrology,
786 161, 423–438.
787 Holland, T.J.B., and Powell, R. (1998) An internally consistent thermodynamic data set for phases of
788 petrological interest. Journal of Metamorphic Geology, 16, 309–343.
789 Holloway, J.R., Dixon, J.E., and Pawley, A. (1992) An internally heated, rapid-quench, high-pressure
790 vessel. American Mineralogist, 77, 643–646.
791 Hooper, A., Ófeigsson, B., Sigmundsson, F., Lund, B., Einarsson, P., Geirsson, H., and Sturkell, E. (2011)
792 Increased capture of magma in the crust promoted by ice-cap retreat in Iceland. Nature Geoscience,
793 4, 783–786.
794 Hreinsdóttir, S., Sigmundsson, F., Roberts, M.J., Björnsson, H., Grapenthin, R., Arason, P., Árnadóttir, T.,
795 Hólmjárn, J., Geirsson, H., Bennett, R.A., and others (2014) Volcanic plume height correlated with
796 magma-pressure change at Grímsvötn Volcano, Iceland. Nature Geoscience, 7, 214–218.
797 Husen, A., Almeev, R.R., and Holtz, F. (2016) The Effect of H2O and Pressure on Multiple Saturation and
798 Liquid Lines of Descent in Basalt from the Shatsky Rise. Journal of Petrology, 57, 309–344.

799 Johnson, K.T.M. (1998) Experimental determination of partition coefficients for rare earth and high-field-
800 strength elements between clinopyroxene, garnet, and basaltic melt at high pressures. Contributions
801 to Mineralogy and Petrology, 133, 60–68.
802 Johnston, A.D. (1986) Anhydrous P-T phase relations of near-primary high-alumina basalt from the South
803 Sandwich Islands - Implications for the origin of island arcs and tonalite-trondhjemite series rocks.
804 Contributions to Mineralogy and Petrology, 92, 368–382.
805 Jude-Eton, T.C., Thordarson, T., Guðmundsson, M.T., and Oddsson, B. (2012) Dynamics, stratigraphy
806 and proximal dispersal of supraglacial tephra during the ice-confined 2004 eruption at Grímsvötn
807 Volcano, Iceland. Bulletin of Volcanology, 74, 1057–1082.
808 Kägi, R., Müntener, O., Ulmer, P., and Ottolini, L. (2005) Piston-cylinder experiments on H_2O
809 undersaturated Fe-bearing systems: An experimental setup approaching fO_2 conditions of natural
810 calc-alkaline magmas. American Mineralogist, 90, 708–717.
811 Keiding, J.K., and Sigmarsson, O. (2012) Geothermobarometry of the 2010 Eyjafjallajökull eruption:
812 New constraints on Icelandic magma plumbing systems. Journal of Geophysical Research: Solid
813 Earth, 117, 1–15.
814 Kelemen, P.B., Joyce, D.B., Webster, J.D., and Holloway, J.R. (1990) Reaction between Ultramafic Rock
815 and Fractionationg Basaltic Magma II: Experimental Investigation of Reaction Between Olivine
816 Tholeiite and Hartburgite at 1150-1050°C and 5 kb. Jour. Petrol., 31, 99–134.
817 Kelemen, P.B., Koga, K.T., and Shimizu, N. (1997) Geochemistry of gabbro sills in the crust-mantle
818 transition zone of the Oman ophiolite: Implications for the origin of the oceanic lower crust. Earth
819 and Planetary Science Letters, 146, 475–488.
820 Kinzler, R.J. (1997) Melting of mantle peridotite at pressures approaching the spinel to garnet transition:
821 Application to mid-ocean ridge basalt petrogenesis. Journal of Geophysical Research: Solid Earth,
822 102, 853–874.
823 Kinzler, R.J., and Grove, T.L. (1992) Primary magmas of mid-ocean ridge basalts 1. Experiments and
824 Methods. Journal of Geophysical Research, 97, 6907.

825 Klügel, A., Hansteen, T.H., and Galipp, K. (2005) Magma storage and underplating beneath Cumbre Vieja
826 volcano, La Palma (Canary Islands). Earth and Planetary Science Letters, 236, 211–226.
827 Kogiso, T., and Hirschmann, M.M. (2001) Experimental study of clinopyroxenite partial melting and the
828 origin of ultra-calcic melt inclusions. Contributions to Mineralogy and Petrology, 142, 347–360.
829 Kogiso, T., Hirose, K., and Takahashi, E. (1998) Melting experiments on homogeneous mixtures of
830 peridotite and basalt: Application to the genesis of ocean island basalts. Earth and Planetary Science
831 Letters, 162, 45–61.
832 Koornneef, J.M., Stracke, A., Bourdon, B., Meier, M.A., Jochum, K.P., Stoll, B., and Grönvold, K. (2012)
833 Melting of a two-component source beneath Iceland. Journal of Petrology, 53, 127–157.
834 Kouchi, A., Sugawara, Y., Kashima, K., and Sunagawa, I. (1983) Laboratory growth of sector zones
835 clinopyroxenes in the system CaMgSi206-CaTiAl206. Contributions to Mineralogy and Petrology,
836 83, 177–184.
837 Laporte, D., Toplis, M.J., Seyler, M., and Devidal, J.-L. (2004) A new experimental technique for
838 extracting liquids from peridotite at very low degrees of melting: Application to partial melting of
839 depleted peridotite. Contributions to Mineralogy and Petrology, 146, 463–484.
840 Lesne, P., Scaillet, B., Pichavant, M., and Beny, J.M. (2011) The carbon dioxide solubility in alkali
841 basalts: An experimental study. Contributions to Mineralogy and Petrology, 162, 153–168.
842 Macdonald, R., Sumita, M., Schmincke, H.U., Bagiński, B., White, J.C., and Ilnicki, S.S. (2015)
843 Peralkaline felsic magmatism at the Nemrut volcano, Turkey: impact of volcanism on the evolution
844 of Lake Van (Anatolia) IV. Contributions to Mineralogy and Petrology, 169.
845 Maclennan, J. (2008) Concurrent mixing and cooling of melts under Iceland. Journal of Petrology, 49,
846 1931–1953.
847 Maclennan, J., McKenzie, D., Grönvold, K., and Slater, L. (2001) Crustal accretion under Northern
848 Iceland. Earth and Planetary Science Letters, 191, 295–310.
849 Maclennan, J., McKenzie, D., Hilton, F., Grönvold, K., and Shimizu, N. (2003a) Geochemical variability
850 in a single flow from northern Iceland. Journal of Geophysical Research, 108, 1–21.

Maclennan, J., McKenzie, D., Grönvold, K., Shimizu, N., Eiler, J.M., and Kitchen, N. (2003b) Melt mixing and crystallization under Theistareykir, northeast Iceland. Geochemistry, Geophysics, Geosystems, 4, 1–40.

Maclennan, J., Gaetani, G.A., Hartley, M.E., Neave, D.A., and Winpenny, B. (2012) Petrological constraints on the crustal structure under rift zones. In AGU Fall Meeting Abstracts p. T41G.

Masotta, M., Mollo, S., Freda, C., Gaeta, M., and Moore, G. (2013) Clinopyroxene-liquid thermometers and barometers specific to alkaline differentiated magmas. Contributions to Mineralogy and Petrology, 166, 1545–1561.

Médard, E., Schmidt, M.W., and Schiano, P. (2004) Liquidus surfaces of ultracalcic primitive melts: Formation conditions and sources. Contributions to Mineralogy and Petrology, 148, 201–215.

Médard, E., McCammon, C.A., Barr, J.A., and Grove, T.L. (2008) Oxygen fugacity, temperature reproducibility, and H2O contents of nominally anhydrous piston-cylinder experiments using graphite capsules. American Mineralogist, 93, 1838–1844.

Meen, J.K. (1990) Elevation of potassium content by fractional crystallization: the effect of pressure. Contributions to Mineralogy and Petrology, 104, 309–331.

Michael, P.J. (1995) Evidence from trace elements and H_2O for regionally distinctive sources of depleted MORB: Implications for evolution of the depleted mantle. Earth and Planetary Science Letters, 131, 301–320.

Mollo, S., Putirka, K.D., Misiti, V., Soligo, M., and Scarlato, P. (2013a) A new test for equilibrium based on clinopyroxene-melt pairs: Clues on the solidification temperatures of Etnean alkaline melts at post-eruptive conditions. Chemical Geology, 352, 92–100.

Mollo, S., Blundy, J.D., Iezzi, G., Scarlato, P., and Langone, A. (2013b) The partitioning of trace elements between clinopyroxene and trachybasaltic melt during rapid cooling and crystal growth. Contributions to Mineralogy and Petrology, 166, 1633–1654.

Moore, G. (2008) Interpreting H2O and CO2 Contents in Melt Inclusions: Constraints from Solubility Experiments and Modeling. Reviews in Mineralogy and Geochemistry, 69, 333–362.

877 Moore, G., and Carmichael, I.S.E. (1998) The hydrous phase equilibria (to 3 kbar) of an andesite and
878 basaltic andesite from western Mexico: constraints on water content and conditions of phenocryst
879 growth. Contributions to Mineralogy and Petrology, 130, 304–319.
880 Moore, G., Roggensack, K., and Klonowski, S. (2008) A low-pressure-high-temperature technique for the
881 piston-cylinder. American Mineralogist, 93, 48–52.
882 Moore, L.R., Gazel, E., Tuohy, R., Lloyd, A.S., Epsosito, R., Steele-MacInnis, M.J., Hauri, E.H., Wallace,
883 P.J., Plank, T., and Bodnar, R.J. (2015) Bubbles matter: An assessment of the contribution of vapor
884 bubbles to melt inclusion volatile budgets. American Mineralogist, 100, 806–823.
885 Müntener, O., Kelemen, P.B., and Grove, T.L. (2001) The role of H2O during crystallization of primitive
886 arc magmas under uppermost mantle conditions and genesis of igneous pyroxenites: an
887 experimental study. Contributions to Mineralogy and Petrology, 141, 643–658.
888 Nakamura, Y. (1973) Origin of sector-zoning of igneous clinopyroxenes. American Mineralogist, 58,
889 986–990.
890 Neave, D.A., Passmore, E., Maclennan, J., Fitton, J.G., and Thordarson, T. (2013) Crystal-melt
891 relationships and the record of deep mixing and crystallization in the AD 1783 Laki eruption,
892 Iceland. Journal of Petrology, 54, 1661–1690.
893 Neave, D.A., Maclennan, J., Hartley, M.E., Edmonds, M., and Thordarson, T. (2014) Crystal storage and
894 transfer in basaltic systems: the Skuggafjöll eruption, Iceland. Journal of Petrology, 55, 2311–2346.
895 Neave, D.A., Maclennan, J., Thordarson, T., and Hartley, M.E. (2015) The evolution and storage of
896 primitive melts in the Eastern Volcanic Zone of Iceland: the 10 ka Grímsvötn tephra series (i.e. the
897 Saksunarvatn ash). Contributions to Mineralogy and Petrology, 170, 1–23.
898 Newman, S., and Lowenstern, J.B. (2002) Volatile Calc: a silicate melt-H_2O-CO_2 solution model written
899 in Visual Basic for excel. Computers and Geosciences, 28, 597–604.
900 Nimis, P. (1995) A clinopyroxene geobarometer for basaltic systems based on crystal-structure modeling.
901 Contributions to Mineralogy and Petrology, 121, 115–125.
902 Parman, S.W., and Grove, T.L. (2004) Harzburgite melting with and without H_2O: experimental data and

predictive modeling. Journal of Geophysical Research, 109, 1–20.

Passmore, E. (2009) Feeding large eruptions: crystallisation, mixing and degassing in Icelandic magma chambers. University of Edinburgh.

Patiño-Douce, A.E., and Beard, J.S. (1996) Effects of P, $f(O_2)$ and Mg/Fe Ratio on Dehydration Melting of Model Metagreywackes. Journal of Petrology, 37, 999–1024.

Pichavant, M., Martel, C., Bourdier, J.-L., and Scaillet, B. (2002) Physical conditions, structure, and dynamics of a zoned magma chamber: Mount Pelée (Martinique, Lesser Antilles Arc). J. Geophys. Res., 107, 2093.

Pickering-Witter, J., and Johnston, A.D. (2000) The effects of variable bulk composition on the melting systematics of fertile peridotitic assemblages. Contributions to Mineralogy and Petrology, 140, 190–211.

Poland, M.P. (2015) "Points Requiring Elucidation" About Hawaiian Volcanism. In R.J. Carey, R.A. Cayley, M.P. Poland, and D. Weis, Eds., Hawaiian Volcanoes: From Source to Surface, Geophysical Monograph, American Geophysical Union pp. 533–562. John Wiley & Sons, Inc., Oxford.

Powell, R., and Holland, T.J.B. (2008) On thermobarometry. Journal of Metamorphic Geology, 26, 155–179.

Putirka, K.D. (1999) Clinopyroxene + liquid equilibria to 100 kbar and 2450 K. Contributions to Mineralogy and Petrology, 135, 151–163.

——— (2008) Thermometers and Barometers for Volcanic Systems. Reviews in Mineralogy and Geochemistry, 69, 61–120.

——— (2016) Amphibole thermometers and barometers for igneous systems, and some implications for eruption mechanisms of felsic magmas at arc volcanoes. American Mineralogist.

Putirka, K.D., Johnson, M., Kinzler, R.J., Longhi, J., and Walker, D. (1996) Thermobarometry of mafic igneous rocks based on clinopyroxene-liquid equilibria, 0–30 kbar. Contributions to Mineralogy and Petrology, 123, 92–108.

Putirka, K.D., Mikaelian, H., Ryerson, F., and Shaw, H.F. (2003) New clinopyroxene-liquid

929 thermobarometers for mafic, evolved, and volatile-bearing lava compositions, with applications to
930 lavas from Tibet and the Snake River Plain, Idaho. American Mineralogist, 88, 1542–1554.
931 Reverso, T., Vandemeulebrouck, J., Jouanne, F., Pinel, V., Villemin, T., Sturkell, E., and Bascou, P. (2014)
932 A two-magma chamber model as a source of deformation at Grímsvötn Volcano, Iceland. Journal of
933 Geophysical Research: Solid Earth, 119, 4666–4683.
934 Robinson, J.A.C., Wood, B.J., and Blundy, J.D. (1998) The beginning of melting of fertile and depleted
935 peridotite at 1.5 GPa. Earth and Planetary Science Letters, 155, 97–111.
936 Rudge, J.F. (2008) Finding peaks in geochemical distributions: A re-examination of the helium-
937 continental crust correlation. Earth and Planetary Science Letters, 274, 179–188.
938 Schwab, B.E., and Johnston, A.D. (2001) Melting Systematics of Modally Variable, Compositionally
939 Intermediate Peridotites and the Effects of Mineral Fertility. J. Petrol., 42, 1789–1811.
940 Scoates, J.S., Lo Cascio, M., Weis, D., and Lindsley, D.H. (2006) Experimental constraints on the origin
941 and evolution of mildly alkalic basalts from the Kerguelen Archipelago, Southeast Indian Ocean.
942 Contributions to Mineralogy and Petrology, 151, 582–599.
943 Shishkina, T.A., Botcharnikov, R.E., Holtz, F., Almeev, R.R., Jazwa, A.M., and Jakubiak, A.A. (2014)
944 Compositional and pressure effects on the solubility of H_2O and CO_2 in mafic melts. Chemical
945 Geology, 388, 112–129.
946 Shorttle, O., and Maclennan, J. (2011) Compositional trends of Icelandic basalts: Implications for short-
947 length scale lithological heterogeneity in mantle plumes. Geochemistry, Geophysics, Geosystems,
948 12, 1–32.
949 Shorttle, O., Moussallam, Y., Hartley, M.E., Maclennan, J., Edmonds, M., and Murton, B.J. (2015) Fe-
950 XANES analyses of Reykjanes Ridge basalts: Implications for oceanic crust's role in the solid Earth
951 oxygen cycle. Earth and Planetary Science Letters, 427, 272–285.
952 Sigmundsson, F., Hreinsdóttir, S., Hooper, A., Arnadóttir, T., Pedersen, R., Roberts, M.J., Óskarsson, N.,
953 Decriem, J., Einarsson, P., Geirsson, H., and others (2010) Intrusion triggering of the 2010
954 Eyjafjallajökull explosive eruption. Nature, 468, 426–430.

Sigurdsson, I.A., Steinthórsson, S., and Grönvold, K. (2000) Calcium-rich melt inclusions in Cr-spinels from Borgarhraun, northern Iceland. Earth and Planetary Science Letters, 183, 15–26.

Singh, S.C., Crawford, W.C., Carton, H., Seher, T., Combier, V., Cannat, M., Pablo Canales, J., Düşünür, D., Escartín, J., and Miranda, J.M. (2006) Discovery of a magma chamber and faults beneath a Mid-Atlantic Ridge hydrothermal field. Nature, 442, 1029–1032.

Sisson, T.W., and Grove, T.L. (1993) Experimental investigations of the role of H_2O in calc-alkaline differentiation and subduction zone magmatism. Contributions to Mineralogy and Petrology, 113, 143–166.

Slater, L., McKenzie, D., Grönvold, K., and Shimizu, N. (2001) Melt generation and movement beneath Theistareykir, NE Iceland. Journal of Petrology, 42, 321–354.

Streeter, R., and Dugmore, A. (2014) Late-Holocene land surface change in a coupled social-ecological system, southern Iceland: A cross-scale tephrochronology approach. Quaternary Science Reviews, 86, 99–114.

Stroncik, N.A., Klügel, A., and Hansteen, T.H. (2009) The magmatic plumbing system beneath El Hierro (Canary Islands): Constraints from phenocrysts and naturally quenched basaltic glasses in submarine rocks. Contributions to Mineralogy and Petrology, 157, 593–607.

Strong, D.F. (1969) Formation of the hour-glass structure in augite. Mineralogical Magazine, 37, 472–479.

Takahahshi, E., Nakajima, K., and Wright, T.L. (1998) Origin of the Columbia River basalts: Melting model of a heterogeneous plume head. Earth and Planetary Science Letters, 162, 63–80.

Tarasewicz, J., White, R.S., Brandsdottir, B., and Schoonman, C.M. (2014) Seismogenic magma intrusion before the 2010 eruption of Eyjafjallajokull volcano, Iceland. Geophysical Journal International, 198, 906–921.

Thomson, A., and Maclennan, J. (2013) The distribution of olivine compositions in icelandic basalts and picrites. Journal of Petrology, 54, 745–768.

Thy, P., Lesher, C.E., Nielsen, T.F.D., and Brooks, C.K. (2006) Experimental constraints on the

Skaergaard liquid line of descent. Lithos, 92, 154–180.

Toplis, M.J., and Carroll, M.R. (1995) An Experimental Study of the Influence of Oxygen Fugacity on Fe-Ti Oxide Stability, Phase Relations, and Mineral-Melt Equilibria in Ferro-Basaltic Systems. Journal of Petrology, 36, 1137–1170.

Tormey, D.R., Grove, T.L., and Bryan, W.B. (1987) Experimental petrology of normal MORB near the Kane Fracture Zone: 22°-25°N, mid-Atlantic ridge. Contributions to Mineralogy and Petrology, 96, 121–139.

Vander Auwera, J., and Longhi, J. (1994) Experimental study of a jotunite (hypersthene monzodiorite): constraints on the parent magma composition and crystallization conditions (P, T, fO2) of the Bjerkreim-Sokndal layered intrusion (Norway). Contributions to Mineralogy and Petrology, 118, 60–78.

Vander Auwera, J., Longhi, J., and Duchesne, J.-C. (1998) A liquid line of descent of the jotunite (Hypersthene monzodiorite) suite. Journal of Petrology, 39, 439–468.

Villiger, S., Ulmer, P., Müntener, O., and Thompson, A.B. (2004) The liquid line of descent of anhydrous, mantle-derived, tholeiitic liquids by fractional and equilibrium crystallization - An experimental study at 1·0 GPa. Journal of Petrology, 45, 2369–2388.

Villiger, S., Ulmer, P., and Müntener, O. (2007) Equilibrium and fractional crystallization experiments at 0.7 GPa; the effect of pressure on phase relations and liquid compositions of tholeiitic magmas. Journal of Petrology, 48, 159–184.

Wallace, P.J., Kamenetsky, V.S., and Cervantes, P. (2015) Melt inclusion CO_2 contents, pressures of olivine crystallization, and the problem of shrinkage bubbles. American Mineralogist, 100, 787–794.

Wasylenki, L.E., Baker, M.B., Kent, A.J.R., and Stolper, E.M. (2003) Near-solidus Melting of the Shallow Upper Mantle: Partial Melting Experiments on Depleted Peridotite. Journal of Petrology, 44, 1163–1191.

Welsch, B., Hammer, J.E., Baronnet, A., Jacob, S., Hellebrand, E., and Sinton, J.M. (2016) Clinopyroxene in postshield Haleakala ankaramite 2. Texture, compositional zoning, and supersaturation in the

magma. Contributions to Mineralogy and Petrology.

Whitaker, M.L., Nekvasil, H., Lindsley, D.H., and Difrancesco, N.J. (2007) The role of pressure in producing compositional diversity in intraplate basaltic magmas. Journal of Petrology, 48, 365–393.

Whitaker, M.L., Nekvasil, H., Lindsley, D.H., and McCurry, M. (2008) Can crystallization of olivine tholeiite give rise to potassic rhyolites? - An experimental investigation. Bulletin of Volcanology, 70, 417–434.

Winpenny, B., and Maclennan, J. (2011) A partial record of mixing of mantle melts preserved in icelandic phenocrysts. Journal of Petrology, 52, 1791–1812.

Wood, B.J., and Blundy, J.D. (1997) A predictive model for rare earth element partitioning between clinopyroxene and anhydrous silicate melt. Contributions to Mineralogy and Petrology, 129, 166–181.

Yang, H.-J., Kinzler, R.J., and Grove, T.L. (1996) Experiments and models of anhydrous, basaltic olivine-plagioclase-augite saturated melts from 0.001 to 10 kbar. Contributions to Mineralogy and Petrology, 124, 1–18.

Yoder, H.J., and Tilley, C.E. (1962) Origin of Basalt Magmas: an Experimental Study of Natural and Synthetic Rocks Systems. Journal of Petrology, 3, 342–532.

Zellmer, G.F., Sakamoto, N., Iizuka, Y., Miyoshi, M., Tamura, Y., Hsieh, H.-H., and Yurimoto, H. (2014) Crystal uptake into aphyric arc melts: insights from two-pyroxene pseudo-decompression paths, plagioclase hygrometry, and measurement of hydrogen in olivines from mafic volcanics of SW Japan. Geological Society, London, Special Publications, 385, 161–184.

Figure 1 Tests performed on published clinopyroxene-liquid barometers with data from experiments carried out on H_2O-poor tholeiites (dark red points). Test data were collated from the following sources: Berndt et al. (2005), Botcharnikov et al. (2008), Grove et al. (1992), Husen et al. (2016), Thy et al. (2006), Toplis and Carroll (1995), Villiger et al. (2004, 2007), Whitaker et al. (2007, 2008) and Yang et al. (1996). One-to-one lines between experimental and calculated pressures are shown in pale grey. Regression lines through the test dataset are shown in black. Data from Villiger et al. (2004, 2007) and composition 70-002 from Grove et al. (1992) that were excluded from the regressions used to summarize barometer performance are shown in grey. The following barometers were tested: (a) model P1 from Putirka et al. (1996), a Jd-in-clinopyroxene barometer; (b) equation 30 from Putirka (2008), a Jd-in-clinopyroxene barometer; (c) equation 32a from Putirka (2008), a clinopyroxene composition barometer; and (d) equation 32c from Putirka (2008), an Al partitioning barometer.

Figure 2 Calibration of a new Jd-in-clinopyroxene barometer. The barometer's abilities to reproduce experimental pressures with (a) imposed and (b) iteratively calculated temperatures are shown, alongside (c) the ability of equation 33 from Putirka (2008) to reproduce experimental temperatures during iterative calculations. The new barometer is directly compared with model P1 from Putirka et al. (1996) in (d). Note that the new barometer faithfully reproduces the pressure of a wider range of 1 atm experiments than model P1 from Putirka et al. (1996).

Figure 3 Tests performed on the new Jd-in-clinopyroxene barometer using a global dataset of clinopyroxene-saturated experiments performed at ≤20 kbar (Bender et al. 1978; Johnston 1986; Kelemen et al. 1990; Meen 1990; Bartels et al. 1991; Vander Auwera and Longhi 1994; Patiño-Douce and Beard 1996; Falloon et al. 1999, 2001; Grove et al. 1997, 2003; Kinzler 1997; Falloon et al. 1997; Gaetani and Grove 1998; Johnson 1998; Kogiso et al. 1998; Robinson et al. 1998; Takahahshi et al. 1998; Vander Auwera et al. 1998; Draper and Green 1999; Pickering-Witter and Johnston 2000; Kogiso and Hirschmann 2001; Müntener et al. 2001; Berndt et al. 2001; Schwab and Johnston 2001; Dann et al.

2001; Pichavant et al. 2002; Bulatov et al. 2002; Wasylenki et al. 2003; Elkins-Tanton and Grove 2003; Barclay 2004; Laporte et al. 2004; Médard et al. 2004; Parman and Grove 2004; Kägi et al. 2005; Scoates et al. 2006; Di Carlo et al. 2006; Ganino et al. 2013). The barometer's abilities to reproduce experimental pressures with (a) imposed temperatures and (b) iteratively calculated temperatures are shown. High-fO_2 experiments on phonolitic compositions that return significantly overestimated pressures are marked (Berndt et al. 2001).

Figure 4 Tests performed on the new Jd-in-clinopyroxene barometer using the same test dataset of experiments performed on H_2O-poor tholeiites plotted in Figure 1. The barometer's abilities to reproduce experimental pressures with (a) imposed temperatures and (b) iteratively calculated temperatures are shown, alongside (c) its ability to reproduce experimental temperatures with equation 33 from Putirka (2008) during iterative calculations. The performance of the new barometer is directly compared with that of model P1 from Putirka et al. (1996) in (d).

Figure 5 A summary of the clinopyroxene compositions used to investigate magma storage pressures under Icelandic rift zones. Clinopyroxene compositions and components were calculated on a six oxygen (6O) basis following the methods outlined in Table 3 from Putirka (2008). Horizontal black bars on (c) and (d) show the lower limits of Al (6O) and Jd considered to represent equilibrium sector zone compositions and reliable analyses respectively. See the main text for further discussion. Unzoned experimental clinopyroxene compositions from Husen et al. (2016) are also shown to aid in the identification of equilibrium sector zone compositions. Low- and high-Al sector zone arrays are also marked on (c).

Figure 6 Kernel density estimates (KDEs) of clinopyroxene Mg# distributions for (a) the full clinopyroxene compilation and (b) clinopyroxene compositions to which equilibrium liquid compositions were successfully matched. KDEs were calculated with a bandwidth comparable to the 1σ precision of

Mg# determinations (±0.5 mol.%). Vertical red lines show the Mg# of clinopyroxenes calculated to be in equilibrium with erupted liquids (see the main text for details). Only whole-rock analyses of groundmass separates, which are an inexact reflection of liquid compositions, were available for the Thjórsá lava (Halldórsson et al. 2008), so a tentative equilibrium clinopyroxene composition is marked with a vertical dashed line. Distinct clinopyroxene populations from the Laki and Thjórsá lavas, and the 10 ka Grímsvötn tephra series are marked with different colors in (b). KDEs of the full clinopyroxene compilation are also shown in pale grey behind the KDEs of matched clinopyroxenes. Matches were found for most clinopyroxene compositions, with the notable exception of the most primitive clinopyroxenes from Borgarhraun ($Mg\#_{cpx} > 90$), which grew from melts that were much more primitive than any known to have erupted in Iceland (Winpenny and Maclennan 2011)

Figure 7 A summary of the clinopyroxene compositions to which equilibrium liquid compositions were successfully matched. Symbols as in Figure 5.

Figure 8 A summary of calculated temperatures and pressures as functions of clinopyroxene Mg# ((a) and (b) respectively) and Al (6O) ((c) and (d) respectively). Regressions through the results are shown in black. The red regression in (b) excludes results from the Borgarhraun lava. Symbols as in Figure 5.

Figure 9 KDEs of pressures and temperatures calculated for the clinopyroxene populations identified in Figure 6b. (a) Pressure KDEs calculated with a bandwidth of 1.4 kbar, which is comparable to the SEE of the new Jd-in-clinopyroxene barometer (Figure 2b). (b) Temperature KDEs calculated with a bandwidth of 17 °C, which is comparable with the SEE of equation 33 from Putirka (2008) when applied to experiments on low-H_2O tholeiites in conjunction with the new barometer (Figure 4c).

Supplementary Figure 1 A comparison of pressures returned from iterative thermobarometric calculations performed on Icelandic clinopyroxene compositions using our new barometer and equation

33 from Putirka (2008), and expressions from Putirka et al. (1996). A one-to-one line and a regression through the calculation results are shown in grey and black respectively.

TABLES

Table 1 A summary of the experimental data used to calibrate the new Jd-in-clinopyroxene barometer

Source	n	Pressure (kbar)	Temperature (°C)	H_2O (wt.%)
Blatter and Carmichael (2001)	13	0.548–2.28	930–1000	3–6
Kinzler and Grove (1992)	30	9–16	1250–1350	anhydrous
Moore and Carmichael (1998)	10	0.441–2.496	950–1075	3–5
Putirka et al. (1996)	23	8–20	1100–1390	anhydrous
Sisson and Grove (1993)	17	1–2	965–1082	3.8–6.2
Yang et al. (1996)	20	0.001	1110–1190	anhydrous

Table 2 Icelandic clinopyroxene data sources

Eruption	Sources
Holuhraun 1 and 2	Hartley and Thordarson (2013)
Laki	Neave et al. (2013)
10 ka Grímsvötn tephra series	Neave et al. (2015)
Skuggafjöll	Neave et al. (2014)
Thjórsá	Passmore (2009)
Borgarhraun	Maclennan et al. (2001), Maclennan et al. (2003a) and Slater et al. (2001)

Table 3 Barometric results and properties of Gaussian fits to pressures calculated for individual clinopyroxene populations

Clinopyroxene population	Mean	1σ	1SEE	$Mean_{Gaussian}$	$1\sigma_{Gaussian}$
Holuhraun 1 and 2	2.4	0.9	0.3	2.4	1.7
Laki, $Mg\#_{cpx} > 80$	3.8	0.6	0.1	3.7	1.5
Laki, $Mg\#_{cpx} < 80$	2.7	1.0	0.2	2.8	1.6
Grímsvötn tephra series, $Mg\#_{cpx} > 80$	3.5	1.0	0.4	3.5	1.6
Grímsvötn tephra series, $Mg\#_{cpx} < 80$	2.9	0.9	0.2	2.8	1.6
Skuggafjöll	3.6	1.3	0.1	3.6	1.8
Thjórsá, $Mg\#_{cpx} > 80$	3.7	1.3	0.4	3.6	1.7
Thjórsá, $Mg\#_{cpx} < 80$	2.6	1.2	0.3	2.5	1.8
Borgarhraun	4.8	1.4	0.1	4.8	1.8

Figure 1

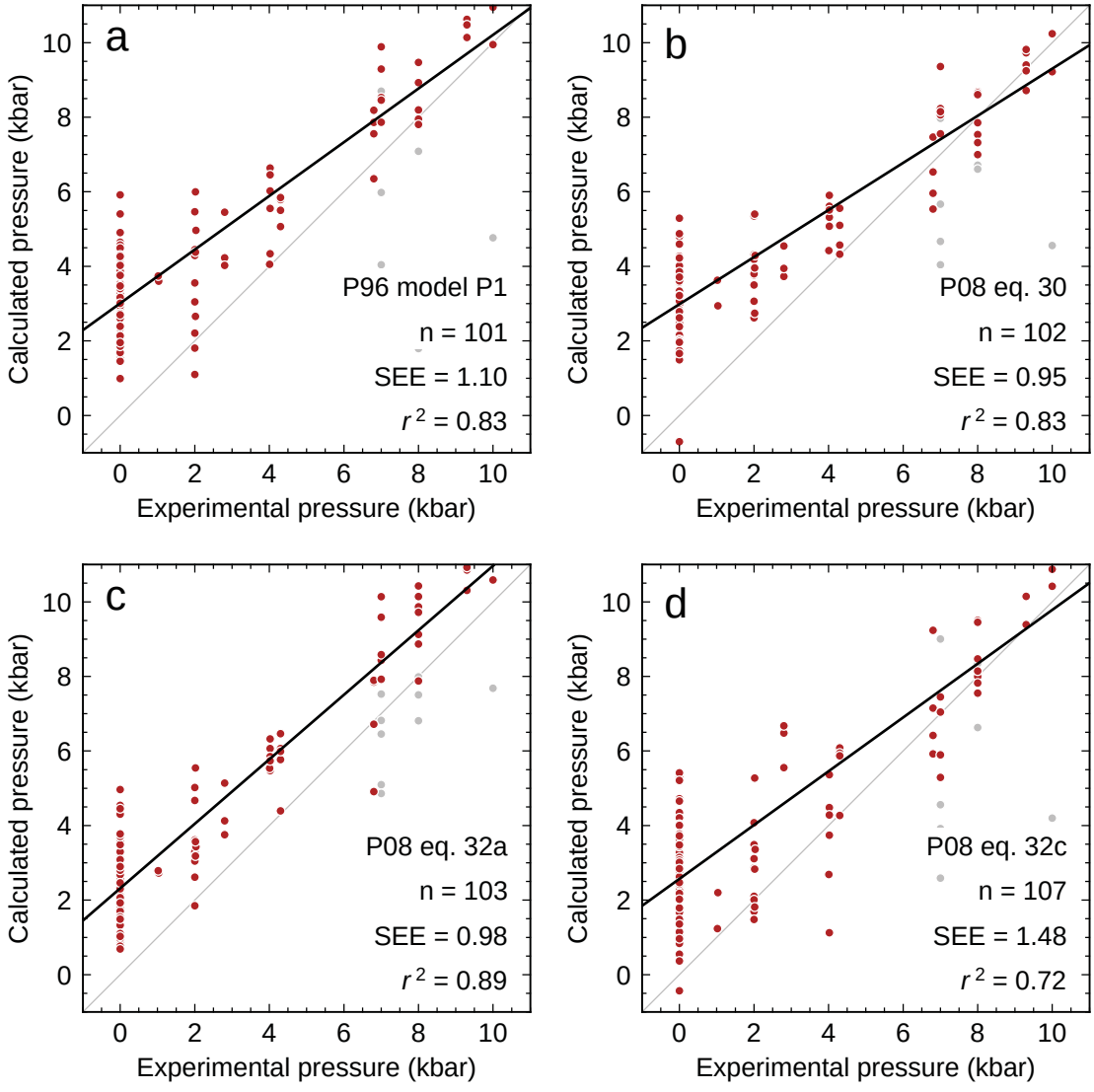
a
P96 model P1
n = 101
SEE = 1.10
r 2 = 0.83
b
P08 eq. 30
n = 102
SEE = 0.95
r 2 = 0.83
c
P08 eq. 32a
n = 103
SEE = 0.98
r 2 = 0.89
d
P08 eq. 32c
n = 107
SEE = 1.48
r 2 = 0.72
Calculated pressure (kbar)
Experimental pressure (kbar)
0
2
4
6
8
10

Figure 2

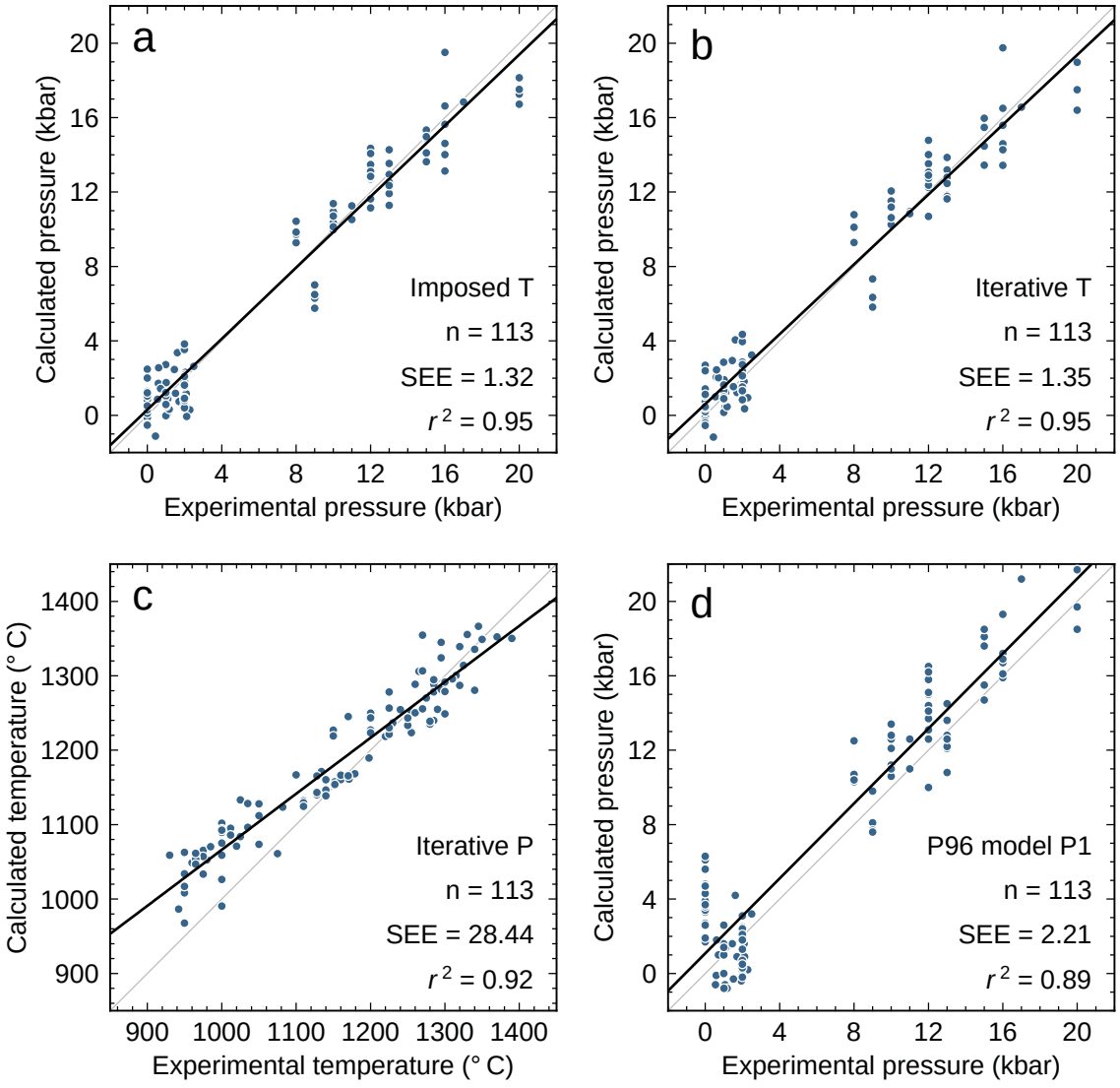
a
Calculated pressure (kbar)
Experimental pressure (kbar)
Imposed T
n = 113
SEE = 1.32
r 2 = 0.95
b
Calculated pressure (kbar)
Experimental pressure (kbar)
Iterative T
n = 113
SEE = 1.35
r 2 = 0.95
c
Calculated temperature (° C)
Experimental temperature (° C)
Iterative P
n = 113
SEE = 28.44
r 2 = 0.92
d
Calculated pressure (kbar)
Experimental pressure (kbar)
P96 model P1
n = 113
SEE = 2.21
r 2 = 0.89

Figure 3

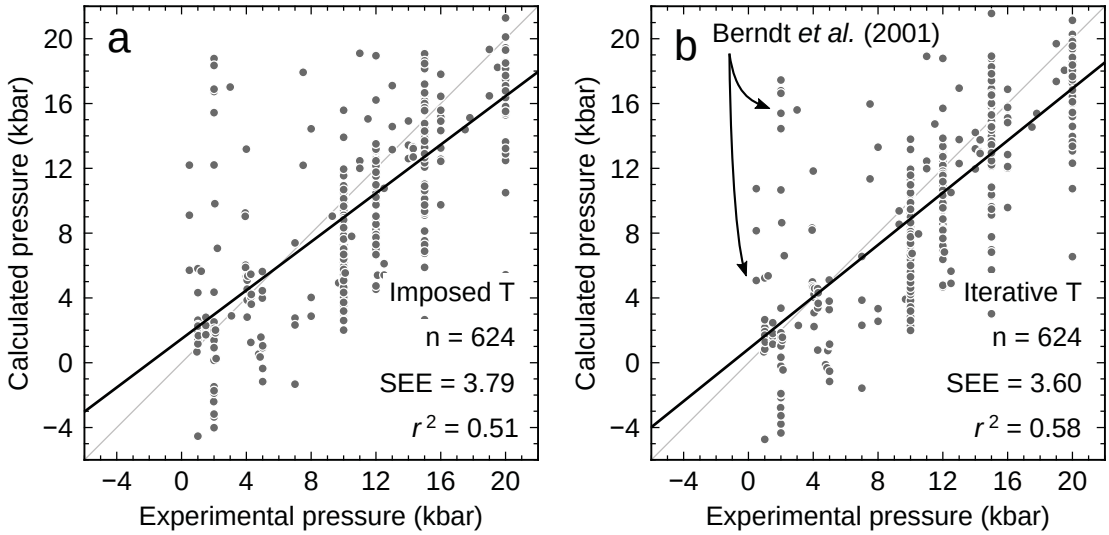
a
Calculated pressure (kbar)
Experimental pressure (kbar)
Imposed T
n = 624
SEE = 3.79
r 2 = 0.51
b
Berndt et al. (2001)
Calculated pressure (kbar)
Experimental pressure (kbar)
Iterative T
n = 624
SEE = 3.60
r 2 = 0.58

Figure 4

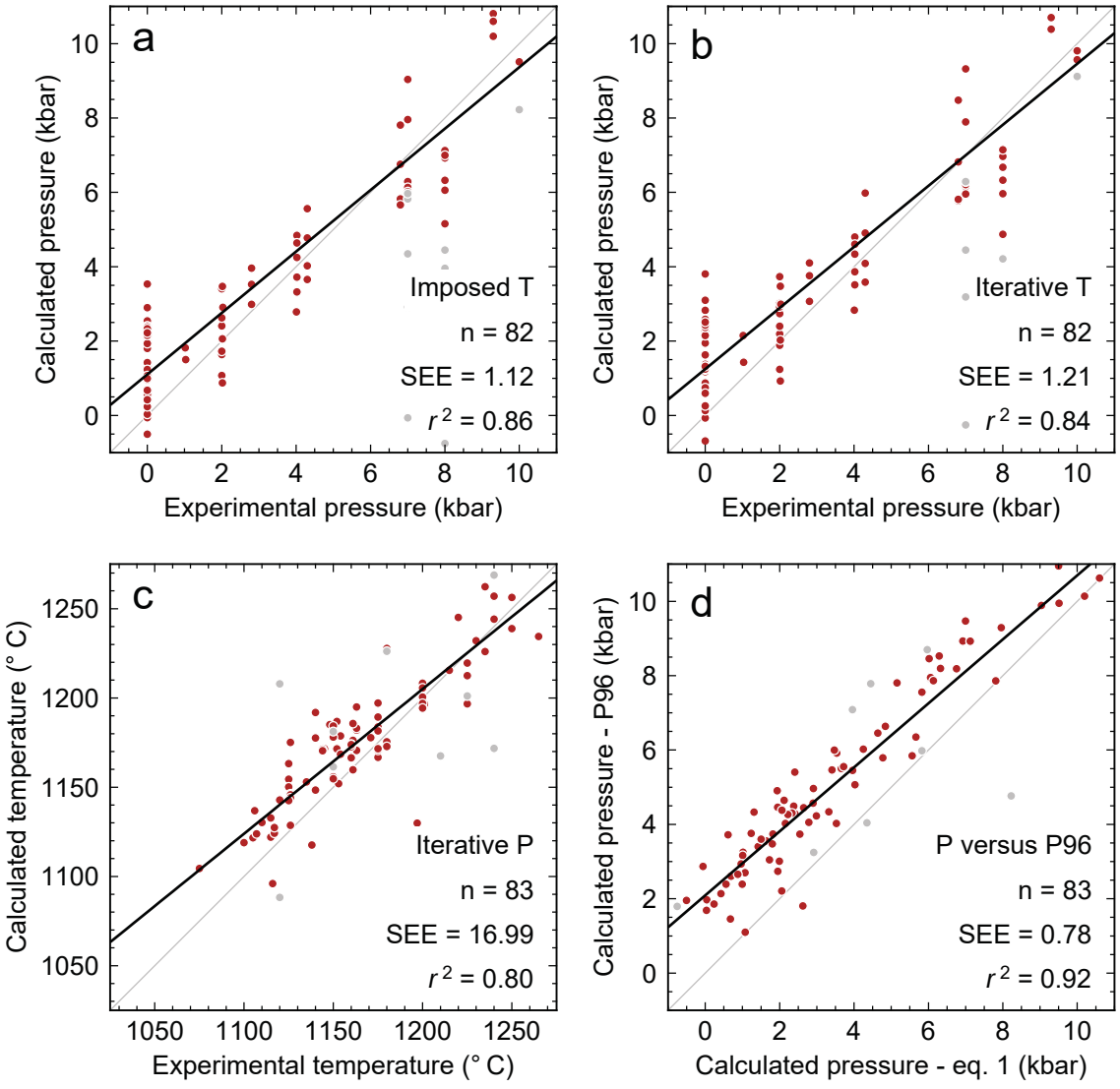
a
Calculated pressure (kbar)
Experimental pressure (kbar)
Imposed T
n = 82
SEE = 1.12
r 2 = 0.86
b
Calculated pressure (kbar)
Experimental pressure (kbar)
Iterative T
n = 82
SEE = 1.21
r 2 = 0.84
c
Calculated temperature (° C)
Experimental temperature (° C)
Iterative P
n = 83
SEE = 16.99
r 2 = 0.80
d
Calculated pressure - P96 (kbar)
Calculated pressure - eq. 1 (kbar)
P versus P96
n = 83
SEE = 0.78
r 2 = 0.92

Figure 5

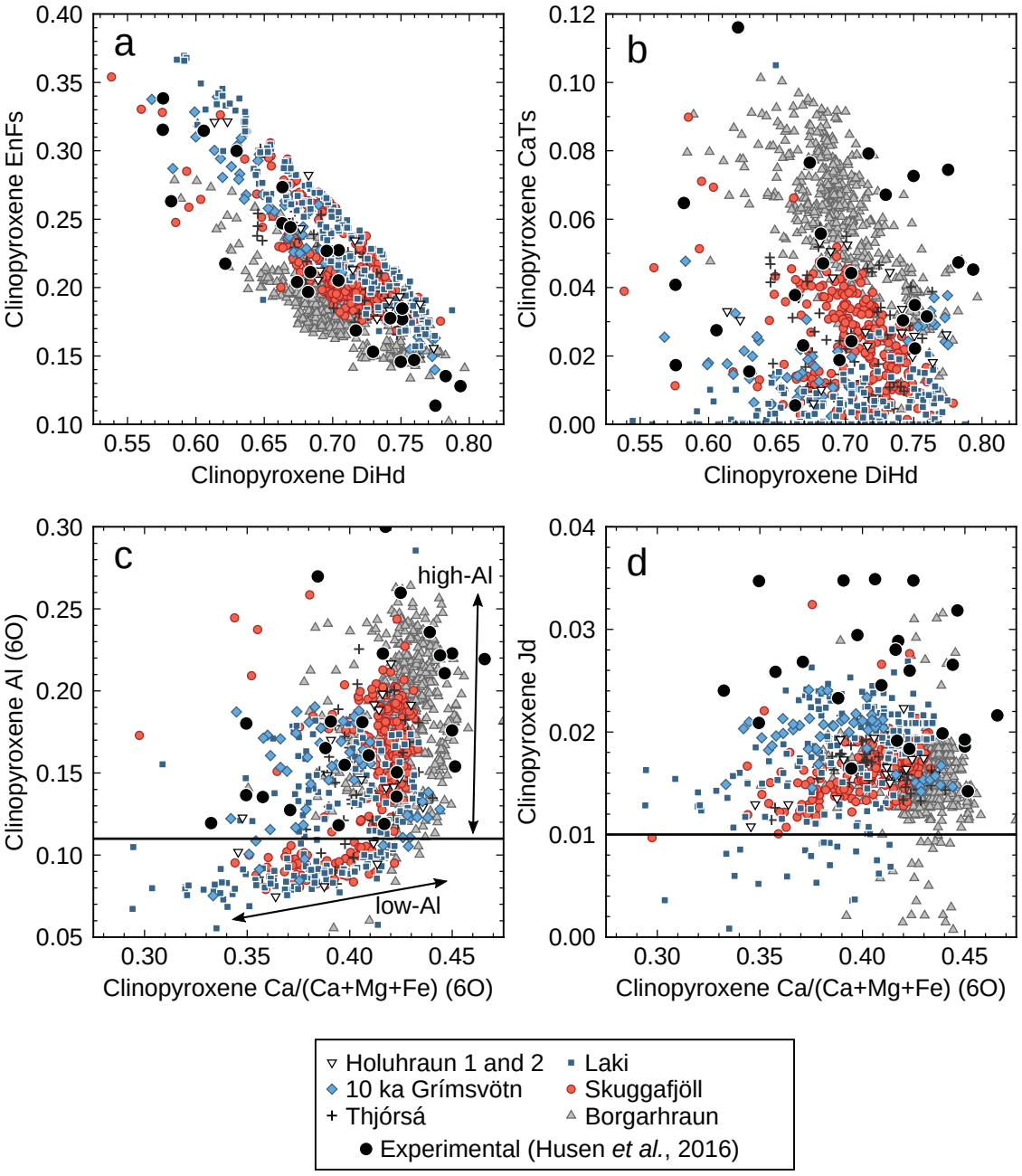
a
b
c
d
Clinopyroxene EnFs
Clinopyroxene DiHd
Clinopyroxene CaTs
Clinopyroxene DiHd
Clinopyroxene Al (6O)
Clinopyroxene Ca/(Ca+Mg+Fe) (6O)
Clinopyroxene Jd
Clinopyroxene Ca/(Ca+Mg+Fe) (6O)
high-Al
low-Al
Holuhraun 1 and 2
Laki
10 ka Grímsvötn
Skuggafjöll
Thjórsá
Borgarhraun
Experimental (Husen et al., 2016)

Figure 6

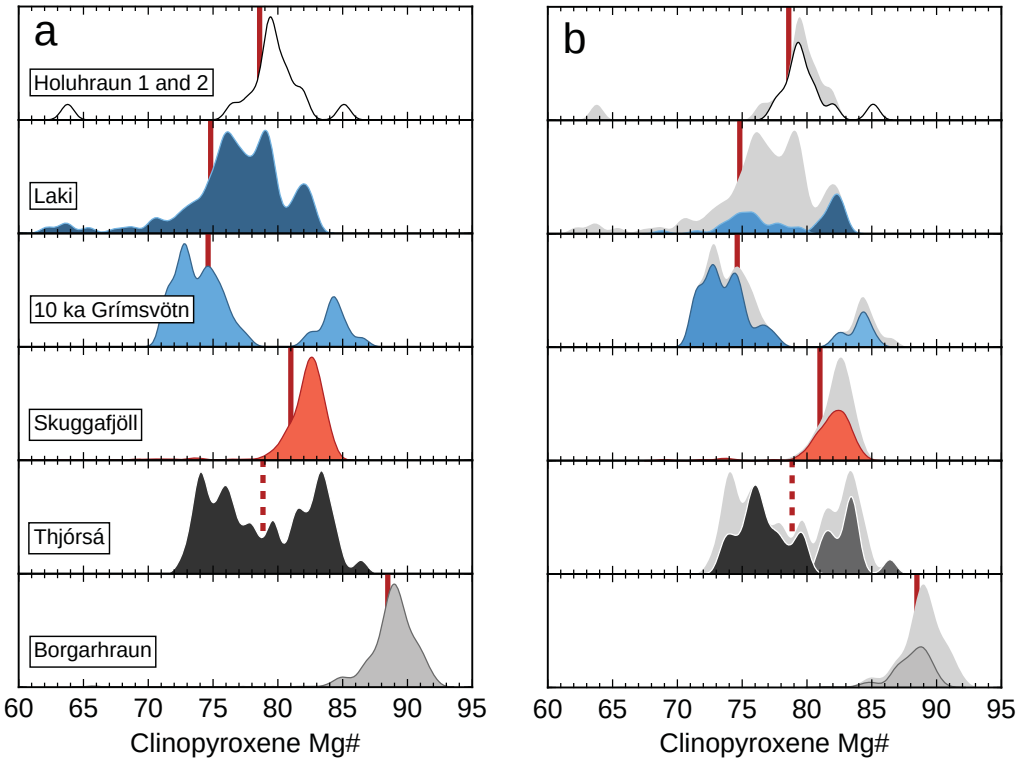
a
Holuhraun 1 and 2
Laki
10 ka Grímsvötn
Skuggafjöll
Thjórsá
Borgarhraun
60 65 70 75 80 85 90 95
Clinopyroxene Mg#
b
60 65 70 75 80 85 90 95
Clinopyroxene Mg#

Figure 7

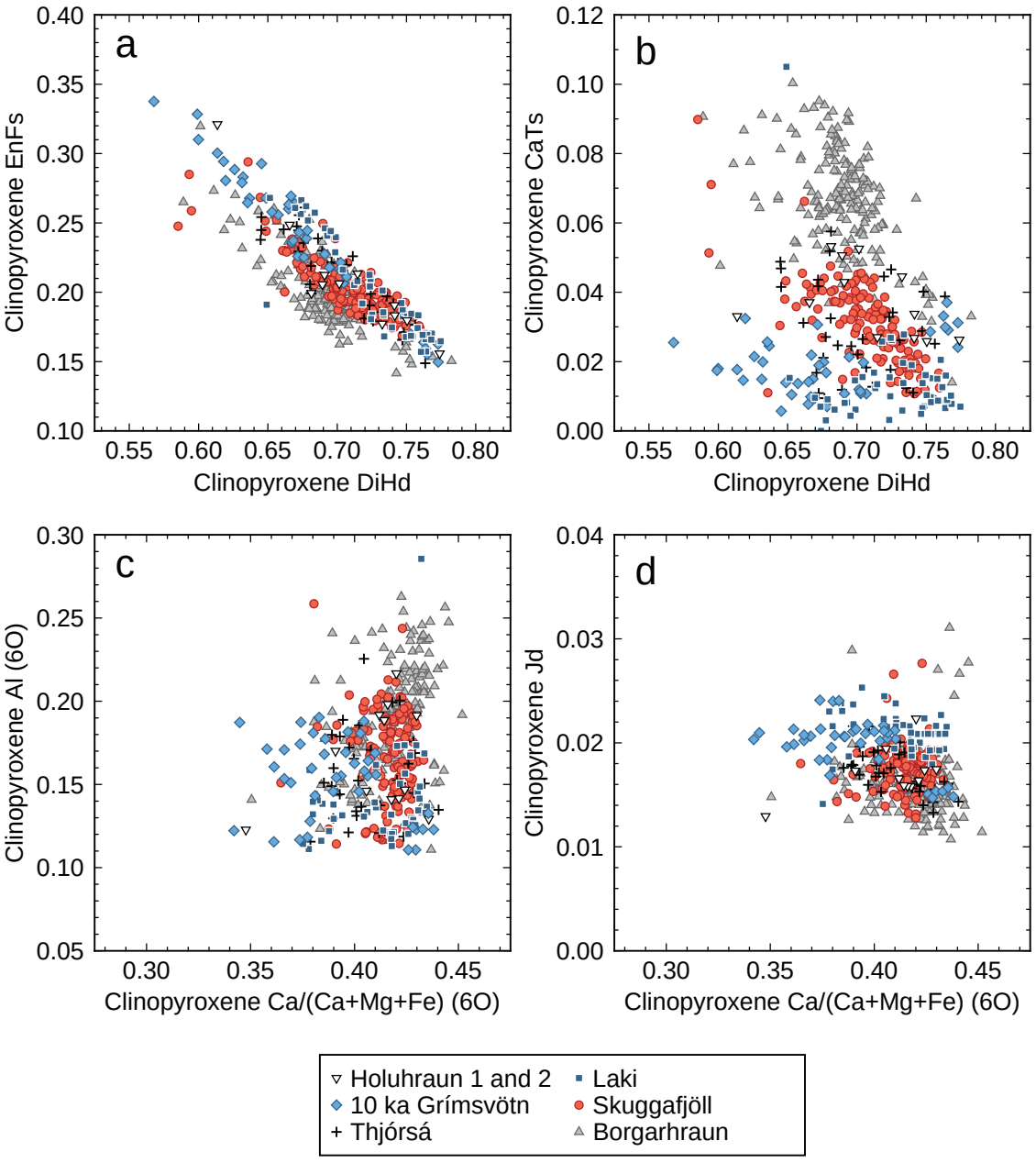
a
b
c
d
Clinopyroxene EnFs
Clinopyroxene CaTs
Clinopyroxene Al (6O)
Clinopyroxene Jd
Clinopyroxene DiHd
Clinopyroxene Ca/(Ca+Mg+Fe) (6O)
0.40
0.35
0.30
0.25
0.20
0.15
0.10
0.12
0.08
0.06
0.04
0.02
0.00
0.05
0.03
0.01
0.55
0.60
0.65
0.70
0.75
0.80
0.30
0.35
0.40
0.45
Holuhraun 1 and 2
10 ka Grímsvötn
Thjórsá
Laki
Skuggafjöll
Borgarhraun

Figure 8

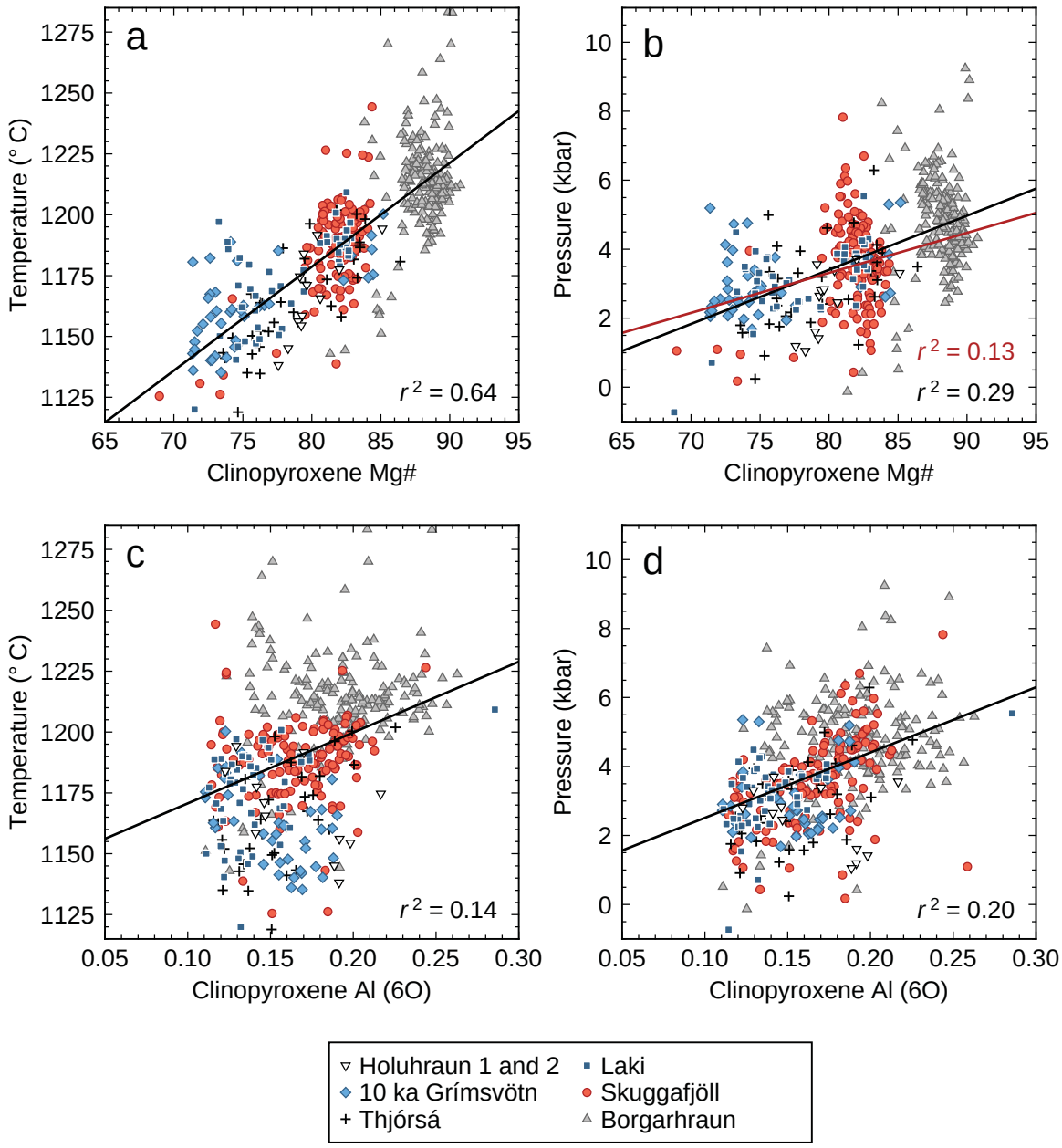
a
b
c
d
Temperature (° C)
Pressure (kbar)
Clinopyroxene Mg#
Clinopyroxene Al (6O)
r 2 = 0.64
r 2 = 0.13
r 2 = 0.29
r 2 = 0.14
r 2 = 0.20
Holuhraun 1 and 2
10 ka Grímsvötn
Thjórsá
Laki
Skuggafjöll
Borgarhraun

Figure 9

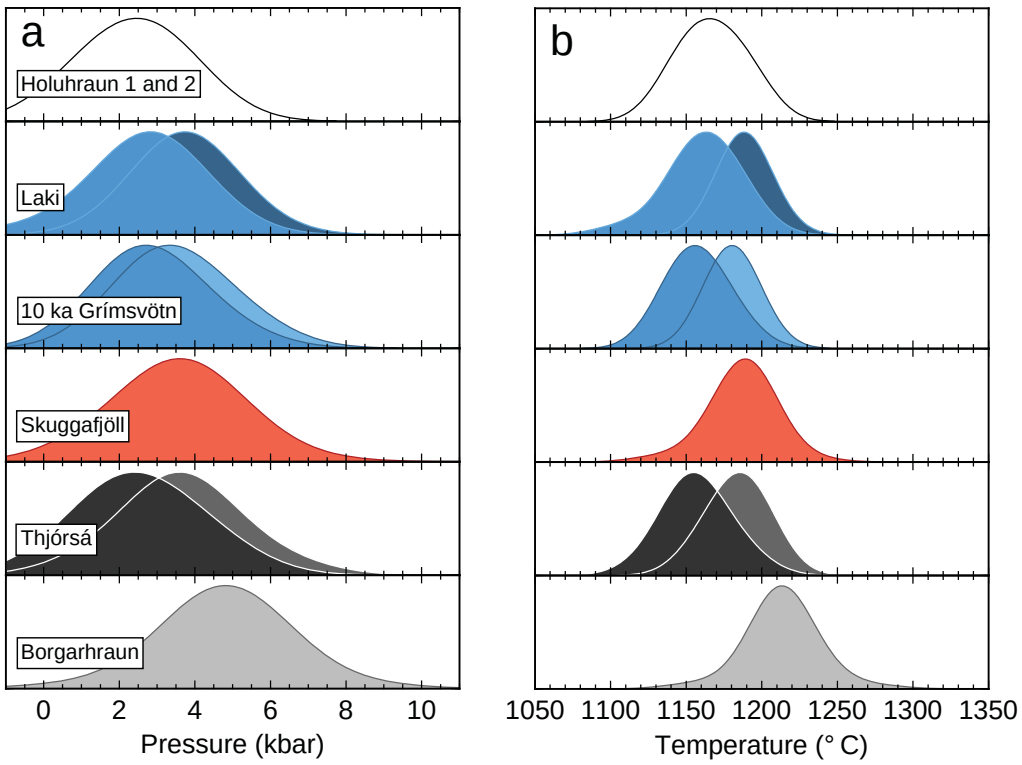
a
Holuhraun 1 and 2
Laki
10 ka Grímsvötn
Skuggafjöll
Thjórsá
Borgarhraun
0
2
4
6
8
10
Pressure (kbar)
b
1050
1100
1150
1200
1250
1300
1350
Temperature (° C)